CANCER

Noncovalently particle-anchored cytokines with prolonged tumor retention safely elicit potent antitumor immunity

Liqian Niu[1], Eungyo Jang[1], Ai Lin Chin[1], Ziyu Huo[1], Wenbo Wang[2], Wenjun Cai[2], Rong Tong[1]*

Preclinical studies have shown that immunostimulatory cytokines elicit antitumor immune responses but their clinical use is limited by severe immune-related adverse events upon systemic administration. Here, we report a facile and versatile strategy for noncovalently anchoring potent Fc-fused cytokine molecules to the surface of size-discrete particles decorated with Fc-binding peptide for local administration. Following intratumoral injection, particle-anchored Fc cytokines exhibit size-dependent intratumoral retention. The 1-micrometer particle prolongs intratumoral retention of Fc cytokine for over a week and has minimal systemic exposure, thereby eliciting antitumor immunity while eliminating systemic toxicity caused by circulating cytokines. In addition, the combination of these particle-anchored cytokines with immune checkpoint blockade antibodies safely promotes tumor regression in various syngeneic tumor models and genetically engineered murine tumor models and elicits systemic antitumor immunity against tumor rechallenge. Our formulation strategy renders a safe and tumor-agnostic approach that uncouples cytokines' immunostimulatory properties from their systemic toxicities for potential clinical application.

INTRODUCTION

Immune checkpoint blockade (ICB) therapy provides long-term remission from numerous cancers in the clinic, but it is ineffective against many tumors that are poorly infiltrated by immune cells, referred to as immune-excluded or immunologically cold tumors (*1*, *2*). These tumors often present a complex network of immunosuppressive pathways, which are unlikely to be overcome by intervention at immune checkpoints alone. Combination immunotherapy that can elicit both innate and adaptive immune responses has been actively pursued to treat immunologically cold tumors (*3*, *4*). Among the many immunostimulatory agents, cytokines are promising for cancer immunotherapy (*5*, *6*). Cytokines, such as interleukin (IL) and interferon (IFN), are potent secretory proteins that provide instructive cues to immune cells (*5*, *7*). Proinflammatory cytokines, such as IL-2 and IL-12, can stimulate innate and adaptive immune cells and can synergize with other immunotherapies by amplifying and coordinating immune cell responses to overcome immunosuppressive tumor microenvironments (TMEs) (*7*). Despite early regulatory approval of IL-2 and IFN-α for cancer treatment (*8*, *9*), the adoption of systemically administered cytokines in the clinic has been hampered by severe dose-limiting toxicity (*10*–*13*); the dose of the cytokines (e.g., IL-2) required to reach therapeutic levels in tumor tissue inevitably overstimulates immune cells in healthy tissues.

The challenges of circumventing systemic exposure of cytokines have been recognized for decades. Tethering cytokines to soluble macromolecules such as poly(ethylene glycol) by means of conventional nonspecific bioconjugation techniques not only can extend the circulation half-time of conjugated cytokines but also results in heterogeneous products that lose structural integrity and activity, and clinical trials of these conjugates [e.g., poly(ethylene glycol)–IL-2] have often been halted because of poor efficacy (*14*). Alternatively, local (intratumoral) administration of cytokines has been studied as a strategy for maximizing their intratumoral retention. However, injected cytokines (e.g., IL-2 and IL-12) enter the systemic circulation within minutes (*11*–*13*, *15*, *16*) owing to their low molecular weights (~10 kDa for IL-2 and ~70 kDa for IL-12). Moreover, intratumoral administration of cytokine-loaded nanoparticles also fails to enhance cytokine retention in tumors (Fig. 1A). For example, 24 hours after intratumoral administration of 150-nm liposomes with IL-2–decorated surfaces, only ~20% of the liposomes remain in the tumor (*17*), whereas intratumoral injection of cytokine-encoding mRNAs encapsulated in lipid nanoparticles results in peak expression of proteins 6 hours after injection, and protein levels gradually decrease thereafter (*18*). Moreover, implantable delivery carriers such as scaffolds and hydrogels fail to prevent cytokines from rapidly entering the circulation within hours (*19*–*25*) because the pores of these carriers (>1 μm) are much larger than cytokine molecules (<10 nm) (*19*).

Another delivery strategy is to link cytokines to collagen-binding peptides for systemic or intratumoral administration, the idea being that peptide binding to collagen in solid tumors would result in retention of the linked cytokines (*26*–*28*). However, 3 days after intratumoral injection, only ~10% of the linked cytokines remain in the tumor (*28*); the poor retention is presumably due to the heterogeneous distribution and turnover of the collagen in tumors. Very recently, IL-12 fused to a phosphorylated alum-binding peptide was engineered and tethered to aluminum hydroxide adjuvant particles for intratumoral administration (*29*). The particles are retained in the tumor for more than a week after intratumoral injection. However, this strategy, as well as many other strategies involving molecularly engineered cytokines (*30*–*33*) and TME-sensitive masked cytokines (*34*–*38*), requires specific protein-engineering techniques and is not universally applicable to all cytokines. Moreover, these sophisticated technologies can be expected to face scale-up problems that will hamper their clinical translation.

[1]Department of Chemical Engineering, Virginia Polytechnic Institute and State University, 635 Prices Fork Road, Blacksburg, VA, 24061, USA. [2]Department of Materials Science and Engineering, Virginia Polytechnic Institute and State University, 445 Old Turner Street, Blacksburg, VA, 24061, USA.
*Corresponding author. Email: rtong@vt.edu

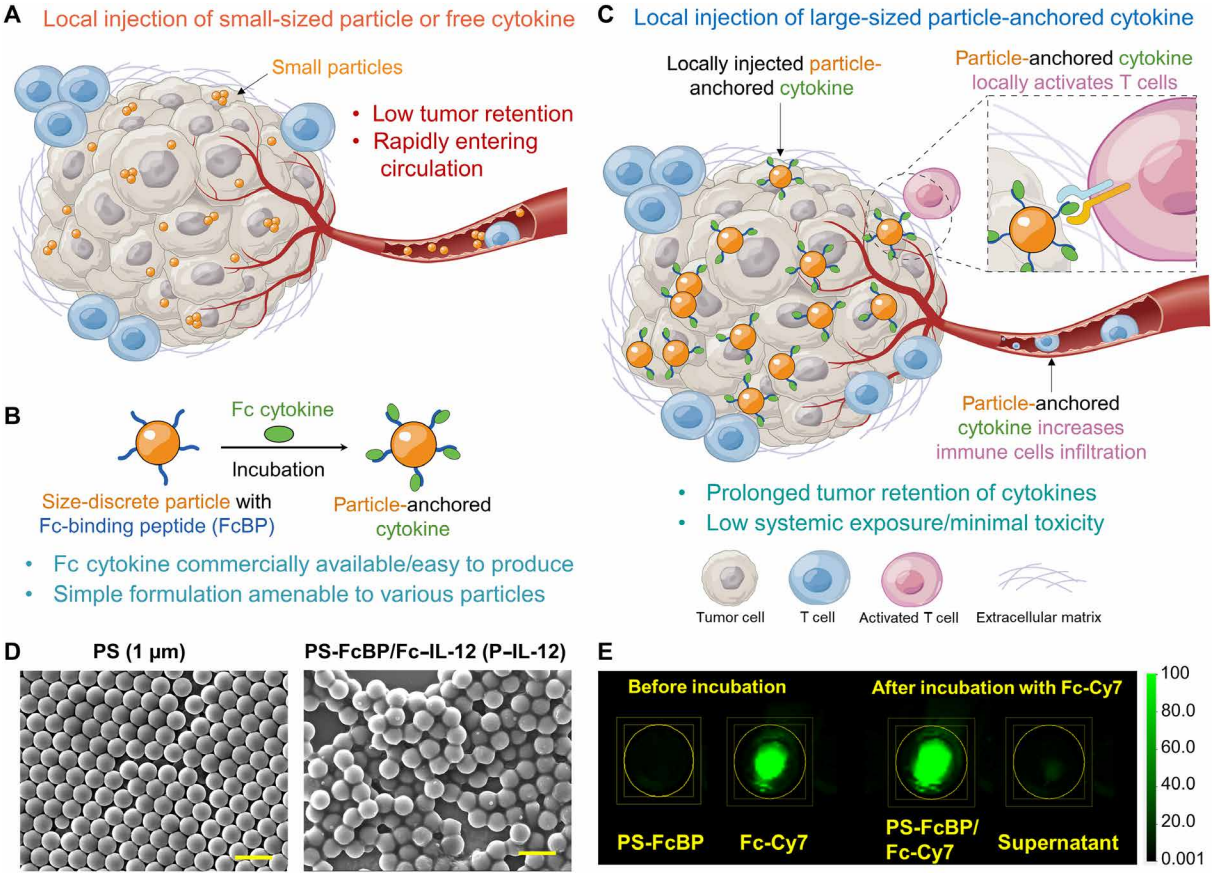

Fig. 1. Design and formulation of a local delivery system using particle-anchored cytokines for cancer immunotherapy. (**A**) Injection of free cytokines or cytokine-loaded nanoparticles into tumors. In both cases, the cytokines quickly enter the systemic circulation owing to leaky tumor vasculature, resulting in systemic toxicity and low therapeutic efficacy. (**B**) Preparation of particle-anchored cytokines by incubation of particles surface-decorated with FcBP with Fc cytokines. (**C**) Increased immune cell infiltration and productive engagement with immune cells (e.g., T cells) due to prolonged tumor retention and minimal systemic toxicity of large (1 μm) cytokine-decorated particles. (**D**) Representative scanning electron microscopy images of PS particles (left) and P–IL-12 (right) after incubating PS-FcBP with Fc–IL-12 and purification. Scale bars, 2 μm. (**E**) Representative fluorescence images for quantification of the formulation process. A mixture of PS-FcBP (no fluorescence) and Fc-Cy7 was incubated for 6 hours and then centrifuged. The separated supernatant rarely exhibited any fluorescence, whereas the pelleted particles showed strong fluorescence (fluorescence quantification is shown in fig. S1C).

Here, we report a facile strategy for noncovalently anchoring commercially available Fc-fused cytokines to the surface of particles decorated with Fc-binding peptide (FcBP) (Fig. 1B). Injection of these particles into tumors resulted in prolonged tumor retention of cytokines with minimal systemic toxicity, and the retention time was particle size dependent (Fig. 1C). Particle-anchored IL-12 (P–IL-12) and P–IL-15 amplified antitumor immunity in immune-excluded tumors. Moreover, when combined with ICB antibodies, these tumor-localized particle-anchored cytokines showed better efficacy than either therapy alone in several syngeneic tumor models and in genetically engineered mouse models.

RESULTS

Fc cytokines can be readily anchored noncovalently to the surface of size-discrete polystyrene particles

In search of a general strategy for easily anchoring cytokines to particles, we developed a formulation that took advantage of the binding between Fc-fused cytokines and FcBP attached to the surface of polystyrene (PS) particles (Fig. 1B). The Fc-fused cytokines were composed of an immunoglobulin G Fc domain linked to a cytokine of interest. Fc-fused proteins are easy to manufacture, and Fc fusion is a widely used strategy for therapeutic proteins (e.g., trastuzumab and cetuximab) (*39*, *40*). Their utility is due to the ability of Fc to improve the solubility and stability of the fused protein, allowing for high protein yields (*40*). We therefore hypothesized that noncovalent binding of the Fc-fused cytokine to the FcBP on the particle surface would not affect the cytokine's structural integrity or bioactivity and that anchoring of the cytokine to particles and subsequent intratumoral injection of the surface-modified particles would enhance local retention of the cytokine to drive tumor growth inhibition while minimizing the systemic exposure of the cytokine, which leads to side effects.

We selected an FcBP with an amino acid sequence of HWRGWV (*41*, *42*), which has a reasonable affinity for Fc even when the peptide is immobilized on beads (K_d = 10 μM) (*42*). A GGGGS spacer was added to the N terminus of the peptide to increase its stability (*43*). We then conjugated the FcBP to carboxylate-functionalized PS

particles using 1-ethyl-3-(3-dimethylaminopropyl)carbodiimide/*N*-hydroxysuccinimide (EDC/NHS) conjugation chemistry (*44*) [~17 μmol of carboxylate per gram of particles (*45*)]. To investigate the effect of particle size on tumor retention, we selected PS particles because they can be prepared in discrete sizes with narrow particle size distributions (for a representative electron microscopy image, see Fig. 1D, left; data of particle size and surface zeta potential in fig. S1, A and B) and they do not aggregate in biological buffers at 37°C. The EDC/NHS conjugation chemistry was chemo-specific in this case because only the N-terminal amine on the FcBP was available for the reaction. After conjugation, the FcBP-decorated PS particles (PS-FcBP) were centrifuged, washed, and then incubated with Cy7-labeled Fc (Fc-Cy7) at room temperature for 6 hours to generate PS-FcBP/Fc-Cy7 particles. The loading efficiency of Fc-Cy7 in these fluorescent particles was determined to be 98% (52 μg of Fc per milligram of PS particles), as indicated by fluorescence imaging (Fig. 1E and fig. S1C), confirming that the FcBP on the particle surface bound strongly to the Fc-Cy7 molecules. We also incubated a mixture of Fc-fused IL-12 (Fc–IL-12) and PS-FcBP at a mass ratio of 1:10 at 4°C for 12 hours to obtain P–IL-12 (data of particle size and surface zeta potential in fig. S1, A and B). An enzyme-linked immunosorbent assay revealed that less than 1% of the Fc–IL-12 remained in the supernatant after centrifugation (fig. S1D), and a scanning electron microscopy image of P–IL-12 indicated the presence of proteins on the particle surface (Fig. 1D, right). Notably, when incubating PS-FcBP/Fc-Cy7 particles in phosphate-buffered saline (PBS) buffer or fetal bovine serum (FBS) cell culture media, we found that less than 2% of Fc-Cy7 was released into the solution and the particle sizes remained unchanged (fig. S1, E and F). These results suggested that our physical binding strategy was suitable for anchoring Fc-fused cytokines onto FcBP-decorated particles.

Particle-anchored cytokines accumulate in tumors in a size-dependent manner and show minimal systemic toxicity

Using large particles for intratumoral drug delivery has been rarely studied, presumably because they are less readily internalized by cells than small particles (*46*–*48*). However, internalization of cytokines is unnecessary because most cytokines initiate and amplify immune responses by engaging with cell surface receptors (*49*). Because tumors have distorted vasculature with leaky pores (>200 nm) (*50*, *51*), we hypothesized that compared with small particles, large particles (>200 nm) would show retarded clearance rates and prolonged tumor retention upon intratumoral administration (Fig. 1C).

To test our hypothesis, we anchored Fc-Cy7 to PS-FcBP particles of various sizes and injected the resulting PS-FcBP/Fc-Cy7 particles into subcutaneous murine 4T1 breast tumors for whole-animal fluorescence imaging studies (Fig. 2A). We found that 1-μm particles remained in the tumors for over 1 week after a single dose (clearance half-life = 91.6 hours), whereas Fc-Cy7 and 200-nm PS-FcBP/Fc-Cy7 particles were quickly cleared (clearance half-lives = 7.1 and 18.9 hours, respectively) (Fig. 2, A and B). Note that FcBP was indispensable for Fc-Cy7 to bind to the particle and be retained in the tumor; in the absence of FcBP, all the Fc-Cy7 was washed off the particles before injection (Fig. 2A, bottom row). One week after intratumoral injection, tumors resected from mice that received 1-μm PS-FcBP/Fc-Cy7 particles showed fluorescence that was 7.7, 13.8, and 17.3 times as strong as that of tumors resected from mice that had been injected with 500- or 200-nm PS-FcBP/Fc-Cy7 particles or with free Fc-Cy7, respectively ($n = 5$, $P < 0.05$ in all cases; Fig. 2, C and D; biodistribution of PS-FcBP/Fc-Cy7 and free Fc-Cy7 7 days after intratumoral injection in fig. S2A). These results collectively demonstrated that 1-μm particles surface-decorated with FcBP showed longer intratumoral retention of Fc-fused molecules than did smaller particles. Note that particles with diameters of ≥2 μm often clogged the needles used for intratumoral injection and were thus not used in this study.

Next, we sought to determine whether intratumoral administration of the particle-anchored cytokines induced systemic toxicity. In clinical trials, patients that receive cytokines, such as IL-12, experience cytokine release syndrome, which is characterized by high concentrations of circulating cytokines, including IFN-γ, that result in side effects (*10*, *13*). Because we used Fc–IL-12 and Fc–IL-15 to treat murine tumors (vide infra), we treated mice bearing B16F10 melanomas with intratumoral administered 1-μm P–IL-12 and P–IL-15 particles (formulated at a dose equivalent to 2 μg of free cytokine) or free Fc–IL-12 and Fc-IL-15 (2 μg of each), and we monitored blood levels of inflammatory cytokines. Over the course of 3 days after intratumoral injection, circulating IL-12 concentrations were significantly lower in mice that received particle-anchored cytokines than in mice that received free cytokines (Fig. 2E, $n = 4$, $P < 0.05$ in all cases). We also observed substantially lower blood IFN-γ concentrations in mice that received the particles, although the IFN-γ concentrations in that group were transiently elevated at 24 hours after injection but had decreased by 3 days after injection (Fig. 2F). Moreover, the tumor necrosis factor–α (TNF-α) and IL-6 concentrations in the P–IL-12 and P–IL-15 group were not significantly higher over 3 days than the concentrations in the other groups (Fig. 2, G and H) nor were the serum concentrations of IL-1α, IL-2, IL-4, and IL-5 at 24 hours after injection (fig. S2, B to E). The transient increase in blood IFN-γ concentration is consistent with literature reports (*29*, *52*, *53*) and can be attributed to the fact that IFN-γ is indispensable for the antitumor efficacy of IL-12 therapy: IL-12 induces IFN-γ release from T cells and natural killer (NK) cells, and IFN-γ, in turn, initiates positive feedback to stimulate T cell activation (*54*). Hematoxylin and eosin staining of heart, lung, kidney, liver, and spleen tissues from mice that received the particle combination regimen did not show any noticeable signs of damage (fig. S3), confirming that the locally administered particle-anchored cytokines did not induce systemic toxicity.

Administration of particle-anchored cytokines and checkpoint blockade antibodies elicits durable antitumor immunity in syngeneic tumor models

We previously reported that sustained local delivery of ICB antibodies to murine tumors by means of photodynamic therapy elicits durable antitumor immunity (*55*). However, this treatment is not curative for poorly immunogenic tumors such as murine 4T1 breast tumors (*56*) or for immune-excluded tumors such as B16F10 melanomas (*57*). In this study, we investigated whether intratumoral administration of P–IL-12 combined with ICB antibodies potentiated the immunotherapeutic activity of the antibodies. We began by testing this combination on mice bearing established subcutaneous 4T1 tumors (50 to 100 mm^3 in volume) at a dosage of once every 6 days for a total of three times (q6d × 3). Intratumoral administration of P–IL-12 (equivalent to 2 μg of Fc–IL-12; ~0.02 mg of particles per dose; for simplicity, all Fc cytokines are hereafter referred by designations that do not include "Fc") in combination with ICB antibodies [anti–cytotoxic T-lymphocyte associated protein 4 (CTLA-4) and anti–programmed cell death-1 (PD-1), each at 50 μg per dose] completely

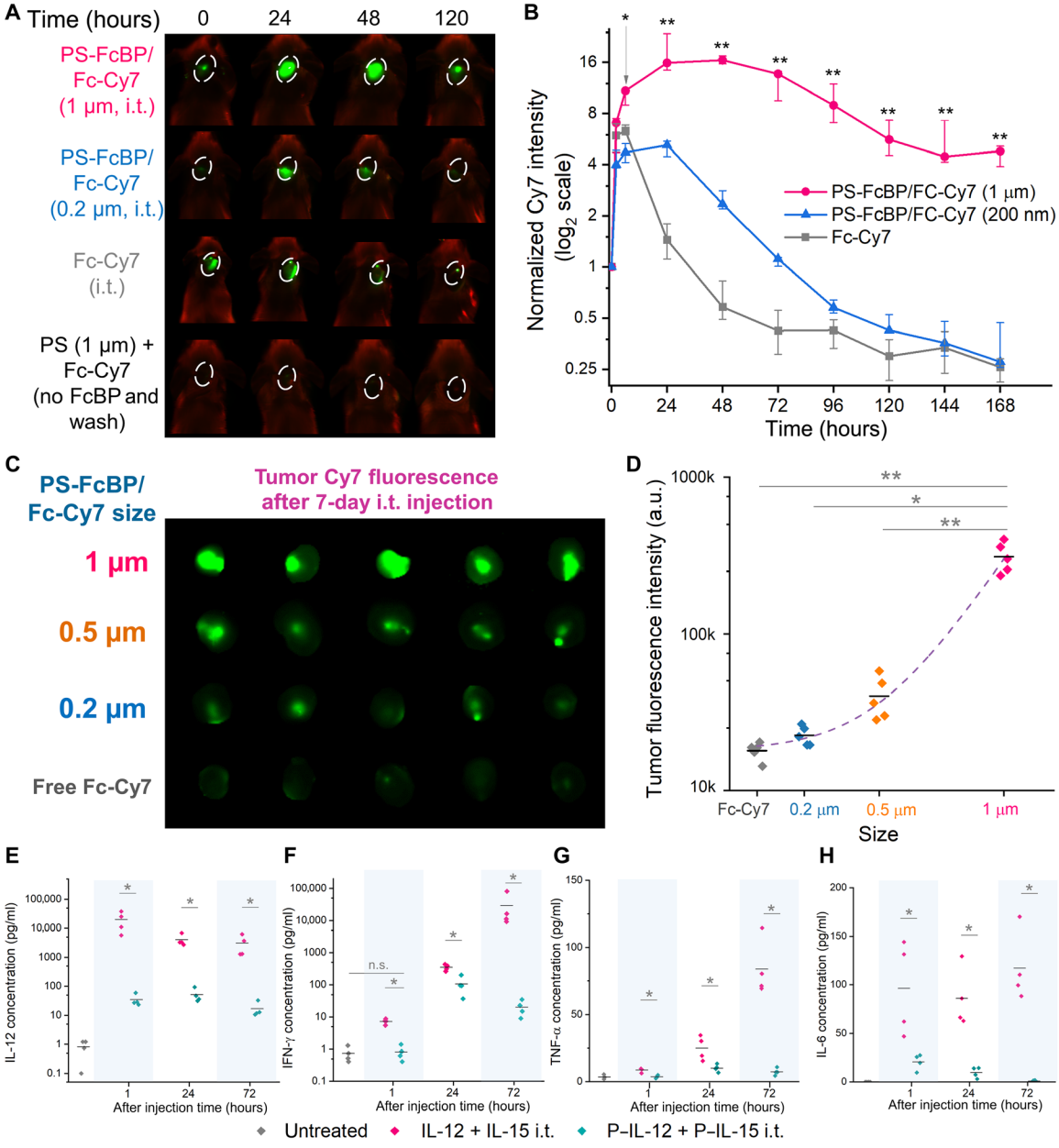

Fig. 2. Particle-anchored Fc molecules exhibit size-dependent intratumoral retention and negligible systemic toxicity after intratumoral administration. (**A**) Representative fluorescence images of 4T1 tumor–bearing mice that received various Fc-Cy7 formulations (Cy7, green) via intratumoral (i.t.) injection. Tumor sites are indicated by white dashed ovals. (**B**) Quantification of changes in Cy7 fluorescence intensity in (A). Data are medians ± quartiles ($n = 4$ or 5). P values were determined by means of a Mann-Whitney U test comparing 1-μm and 200-nm PS-FcBP/Fc-Cy7 particles. (**C**) Fluorescence images of resected 4T1 tumors injected with PS-FcBP/Fc-Cy7 particles of various sizes or with free Fc-Cy7. The tumors were resected on day 7 after injection. (**D**) Quantification of fluorescence intensities of tumors in (C). (**E** to **H**) Temporal dependence of serum concentrations of IL-12 (E), IFN-γ (F), TNF-α (G), and IL-6 (H) after intratumoral injection of B16F10 tumor–bearing mice with P–IL-12 + P–IL-15 (2 μg for each cytokine) ($n = 4$ for each group). Results for other serum biomarkers are shown in fig. S2 (B to E). P values in (D) to (H) were calculated by means of Mann-Whitney U tests. *$P < 0.05$ and **$P < 0.01$. n.s., not significant; a.u., arbitrary units.

eradicated 4T1 tumors, curing all the tumor-bearing mice over the course of 60 days (Fig. 3, A and B; see fig. S4 for a representative histology image of a 4T1 tumor 5 days after intratumoral injection with P–IL-12 and ICB antibodies). In contrast, intraperitoneally administered ICB antibodies, intratumoral IL-12, or intratumoral P–IL-12 alone showed only modest therapeutic effects ($P = 0.0027$, 0.0015, and 0.0026, respectively; $n = 5$ to 7). The intratumoral administration of ICB antibodies and IL-12 resulted in early tumor regression but did not completely eliminate the tumors (Fig. 3, A and B, $P = 0.0019$). The intratumoral combination regimen did not cause body weight loss, whereas a >4% loss in body weight was observed in mice that received intratumoral IL-12 and ICB antibodies ($P = 0.016$ at day 13; Fig. 3C). These results confirmed that the 1-μm IL-12–decorated particles safely potentiated ICB immunotherapy.

In addition, mice cured of 4T1 tumors by the combination regimen rejected rechallenge by subcutaneous inoculation with 5×10^5

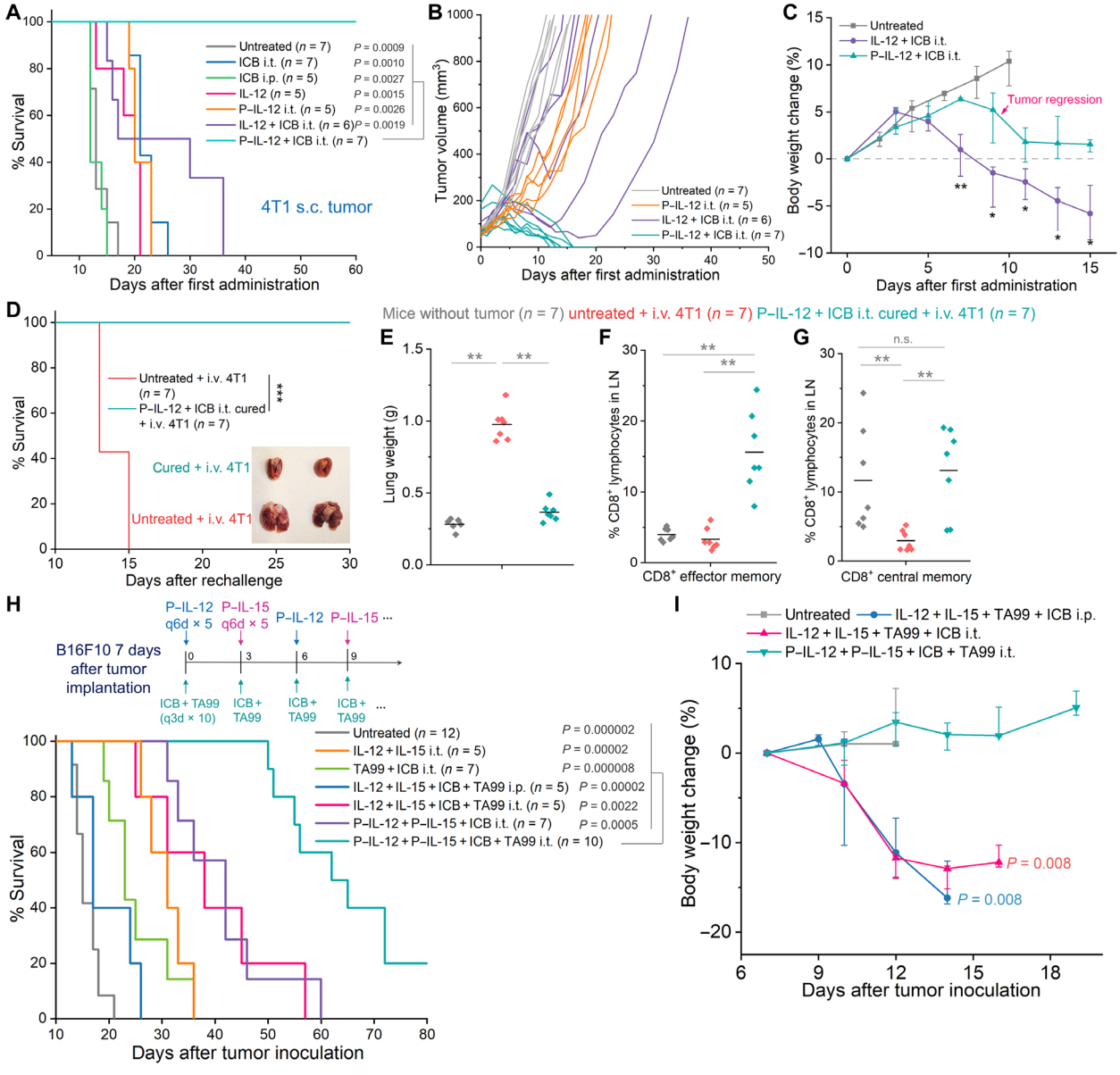

Fig. 3. Particle-anchored cytokines potentiate ICB antibodies in syngeneic tumor models and show minimal systemic toxicity. (**A**) Overall survival curve for balb/c mice inoculated with 5×10^5 4T1 tumor cells and subjected to various treatments (q6d × 3 in all cases) starting when tumor volumes reached ~50 to 100 mm^3 ($n = 5$ to 7). (**B**) Tumor growth curves for selected treatments shown in (A). (**C**) Body weight changes for selected treatments shown in (A). *P* values were determined by means of Mann-Whitney *U* tests for comparisons between the group that received intratumoral IL-12 + ICB antibodies and the group that received intratumoral P–IL-12 + ICB antibodies. (**D**) Survival curves for untreated balb/c mice and cured mice in (A) that received intratumoral P–IL-12 + ICB. All mice were injected with 5×10^5 4T1 cells via the tail vein. Inset shows representative images of lungs from the two groups of mice at the end of the treatment period. i.v., intravenous. (**E**) Comparison of lung weights of mice without tumors and the two groups of mice in (D) ($n = 7$). (**F** and **G**) Fractions of $CD44^{hi}CD62L^{lo}$ effector memory (F) and $CD44^{hi}CD62L^{hi}$ central memory (G) $CD8^+$ T cells in lymph nodes (LNs) of mice in (E). (**H**) Overall survival curves for C57BL/6 mice inoculated with 5×10^5 B16F10 tumor cells and subjected to various treatments starting on day 7 after tumor inoculation ($n = 5$ to 12). i.p., intraperitoneal. (**I**) Body weight changes of selected groups in (H). *P* values were calculated for comparison of the individual group with the group that received P–IL-12 + P–IL-15 + ICB antibodies + TA99. Survival percentages in (A), (D), and (H) were compared by log-rank test. All other *P* values were determined by means of Mann-Whitney *U* tests. $^*P < 0.05$, $^{**}P < 0.01$, and $^{***}P < 0.001$.n.s., not significant.

4T1 cells (fig. S5A). Moreover, on day 90, the fraction of effector memory $CD8^+$ T cells in the lymph nodes of the mice that had rejected the rechallenge was significantly higher than the fraction in untreated mice ($P = 0.0025$, $n = 5$ to 7; fig. S5B), suggesting that intratumoral treatment with the combination regimen induced the formation of effective systemic immune memory.

To investigate whether intratumoral treatment with our combination regimen could effectively control disseminated metastases, we intravenously injected 5×10^5 4T1 tumor cells into mice that had been cured by the combination therapy and then assessed the antimetastasis effect of the therapy. All the mice that had been cured survived for more than 4 weeks ($n = 7$; Fig. 3D). No lung metastases were detected

in these rechallenged mice (representative lung images are shown in Fig. 3D, and representative histology images of lung tissues are shown in fig. S5C), and the lung weights of these mice were lower than those of untreated mice that received intravenous 4T1 cells ($P = 0.0021$, $n = 7$; Fig. 3E). Furthermore, the fractions of effector memory and central memory $CD8^+$ T cells in the lymph nodes of the rechallenged mice were significantly higher than the fraction in untreated mice that received intravenous 4T1 cells, demonstrating that the combination therapy indeed led to long-term immunological memory against disseminated tumor cells ($P = 0.0021$ and 0.0049, respectively, $n = 7$; Fig. 3, F and G) (*58*, *59*).

Encouraged by the synergy between P–IL-12 and ICB antibodies that was observed in the 4T1 tumors, we next explored the combination therapy for treatment of aggressive, immune-excluded B16F10 tumors. Subcutaneously injected B16F10 tumor cells (5×10^5) were allowed to grow for 7 days (at which point their volumes were ~50 mm^3) and were then subjected to various treatments. We found that injection of the B16F10 tumor–bearing mice with the combination of P–IL-12 and ICB antibodies modestly slowed tumor growth ($P = 0.000006$ for comparison with growth in untreated mice, $n = 9$ to 12, q6d × 5; fig. S6A). Similar results were observed for the combination of P–IL-2 and ICB antibodies (fig. S6A).

In an attempt to achieve better therapeutic efficacy, we combined P–IL-15 with an antibody against tyrosinase-related protein–1 (anti–TYRP-1, referred to as TA99) for intratumoral administration. IL-15, a member of the IL-2 superfamily cytokines, has been shown to enhance antitumor immunogenicity when combined with IL-12 (*60*–*63*). Notably, IL-15 does not activate immunosuppressive regulatory T cells (T_{reg} cells), and it less likely causes capillary leak syndrome than IL-2 does (*64*). In addition, TA99 has been shown to slow the growth of B16F10 tumors (*65*). Specifically, we treated mice bearing subcutaneous B16F10 melanomas with a combination of P–IL-12 (q6d × 5), P–IL-15 (q6d × 5), ICB antibodies (q3d × 10), and TA99 (q3d × 10; 2 μg of each cytokine; 100 μg of TA99 per dose; anti–CTLA-4 and anti–PD-1, each at 50 μg/dose; treatment schedule is shown in Fig. 3H). We found that intratumoral administration of this combination therapy significantly delayed tumor growth and enhanced survival, with 2 of 10 mice showing complete tumor regression over 80 days (Fig. 3H). Mice cured by the combination therapy developed vitiligo at the tumor site (fig. S6B), which reportedly indicates an antimelanocyte T cell response (*66*). In contrast, treatment with a combination of free IL-12, IL-15, TA99, and ICB antibodies, either intraperitoneally or intratumorally at the same dosage, did not result in significantly better survival (Fig. 3H, $P = 0.00002$ and 0.0022, respectively, $n = 5$ to 10). TA99 was found to be a necessary component of the combination therapy, as indicated by comparison with survival in a group that received all the other components but no TA99 (Fig. 3H, $P = 0.0005$, $n = 7$ to 10). Notably, despite the high response rates, the combination therapy had minimal systemic toxicity, as indicated by comparison of body weight changes in the group of mice that received intraperitoneal or intratumoral IL-12, IL-15, TA99, and ICB antibodies with the body weights in the other groups ($P = 0.008$, $n = 5$ in all cases; Fig. 3I).

Combination therapy including particle-anchored cytokines enhances tumor immune infiltration and stimulates antitumor immunity

To understand the cellular and molecular mechanisms underlying the observed therapeutic effect of the combination therapy, we sought to determine the contributions of various types of immune cells and soluble factors to therapeutic efficacy in both 4T1 and B16F10 tumor models. Quantification of cytokines and chemokines in 4T1 tumor lysates by means of a Luminex assay revealed six clusters of proteins 5 days after a single administration of various treatments (proteins were clustered by the *K*-means method, $n = 5$ or 6; Fig. 4A). Clusters 1 and 2 consisted of the proinflammatory effector proteins including TNF-α, IFN-γ, CXCL2, CXCL5, IL-1α, IL-6, IL-23, and CCL5, the magnitude of changes in the protein levels of which were higher in mice that received P–IL-12 and ICB antibodies than those in mice that received either IL-12 or ICB antibodies alone; this result indicated a T helper 1–biased TME transformation in the former group (*67*).

To investigate how these proinflammatory effectors affected the TME, we analyzed cellular infiltrates in the treated 4T1 tumors by means of flow cytometry. The fractions of $CD8^+CD3^+$ and $CD4^+CD3^+$ effector T cells (T_{eff} cells) and NK cells in the tumor-infiltrating lymphocytes (TILs) in mice that received the combination therapy were higher than the fractions in untreated mice and mice that received only intratumoral ICB antibodies or IL-12 (Fig. 4, B to D, $n = 6$ to 8; cell population numbers are shown in fig. S7). Notably, we found significantly higher fractions of $CD8^+$ TILs exhibiting an effector memory phenotype ($CD44^{hi}CD62L^{lo}$) in mice that received the combination therapy (Fig. 4E; fractions of central memory $CD8^+$ in TILs in fig. S8A). In addition, the fraction of immunosuppressive $CD4^+CD25^+Foxp3^+$ T_{reg} cells in total $CD4^+$ TILs was significantly lower in mice that received the combination therapy than in the other groups (Fig. 4F). The ratios between T_{eff} cell and immunosuppressive cell populations, specifically, the ratios of $CD8^+$ T_{eff} cells to T_{reg} cells, $CD8^+CD44^+$ cells to T_{reg} cells, and $CD8^+$ T_{eff} cells to myeloid-derived suppressor cells (MDSCs) ($CD11b^+Ly6G^-Ly6C^{hi}$; the fractions of MDSCs in TILs in fig. S8B), were substantially higher in mice that received the combination therapy than in the other groups (Fig. 4, G to I). Tumors treated with the combination therapy had a lower fraction of infiltrating macrophages than did untreated tumors or tumors treated with either IL-12 or ICB antibodies (Fig. 4J). In vivo IL-12 reportedly alters the macrophage profiles in 2 hours, increasing the production of proinflammatory cytokines (*68*), a behavior that might be attributable to the reduction in the fraction of macrophages in TILs (numbers of macrophages per milligram of tumor are shown in fig. S7E). Moreover, the combination therapy induced substantial increases in the fractions of dendritic cells (Fig. 4K), $CD8^+$ effector memory and central memory T cells, and B cells in the lymphocytes in tumor-draining lymph nodes (fig. S8, C to E). Together, these findings suggested that the combination therapy stimulated antitumor immune responses, enhanced infiltration of effector cells into tumors, and attenuated the population of immunosuppressive cells, thereby contributing to the therapeutic effects observed in Fig. 3A.

We next evaluated how the combination of P–IL-12, P–IL-15, ICB antibodies, and TA99 affected the infiltration of TILs in immune-excluded B16F10 tumors. The trends were similar to what was observed in 4T1 tumors (Fig. 4A). Specifically, 7 days after injection of the combination therapy, the fractions of various proinflammatory cytokines [i.e., TNF-α, IFN-γ, IL-1β, IL-12p70, IL-18, and granulocyte-macrophage colony-stimulating factor (GM-CSF); cluster 1 in Fig. 5A] were found to be up-regulated. Seven days after treatment, flow cytometry analysis of TILs in the B16F10 tumors showed that compared with untreated mice and mice that received free cytokines or

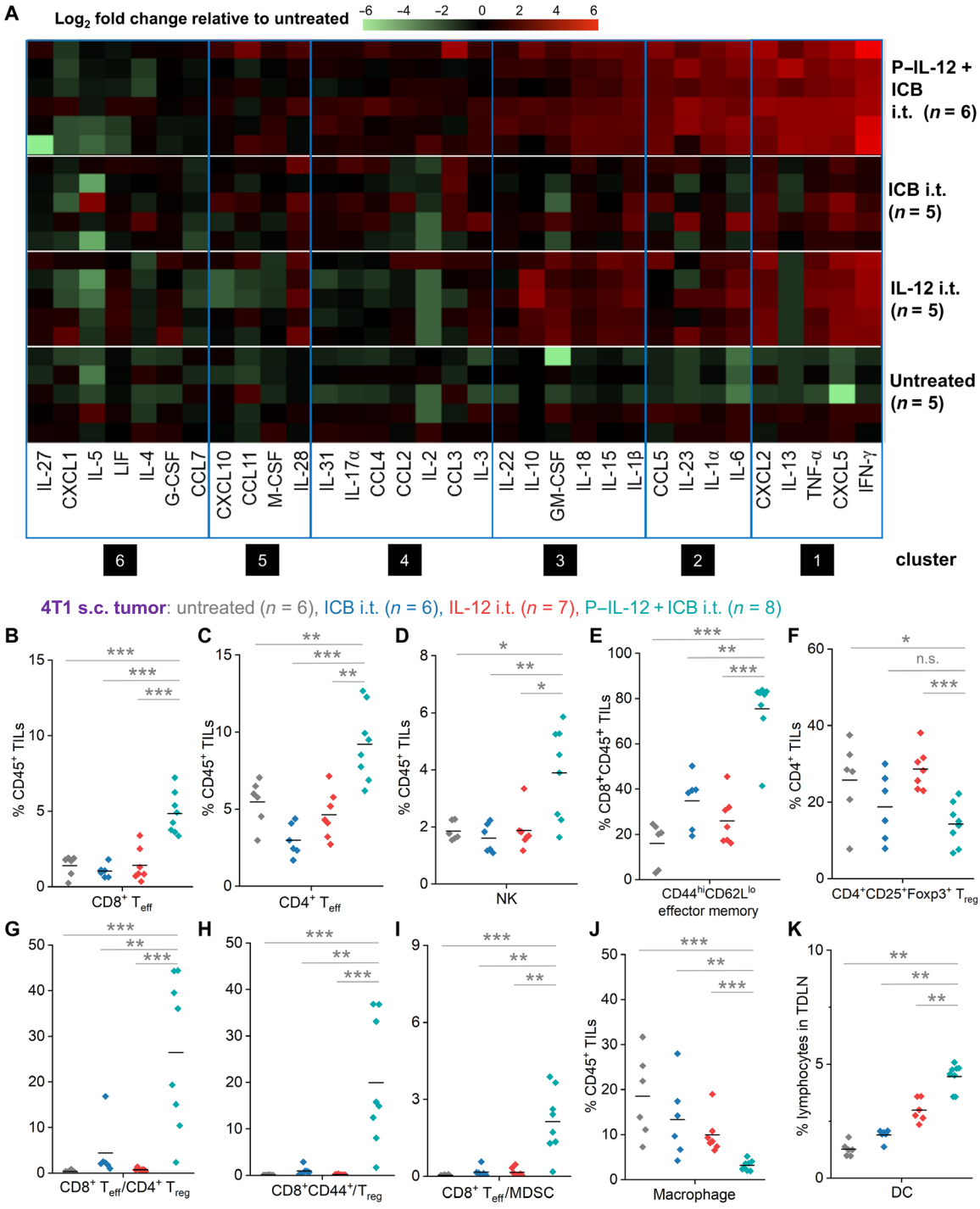

Fig. 4. Intratumoral administration of a combination of P–IL-12 and ICB antibodies induces inflammatory TMEs and affects immune cell infiltration into 4T1 tumors. (**A**) Luminex assay of cytokine and chemokine levels in 4T1 tumor–bearing mice treated with the indicated therapies. On day 5 following intratumoral treatment, tumors were isolated, and cytokine and chemokine levels were assayed (n = 5 to 6). The chemokines and cytokines were clustered by the K-means method. (**B** to **K**) Flow cytometry analysis of lymphocytes in untreated 4T1 tumor–bearing mice and mice that received ICB antibodies, IL-12, or a combination of P–IL-12 and ICB antibodies. Tumors were collected on day 5 after treatment (n = 6 to 8). (B) Fractions of $CD8^+CD3^+T_{eff}$ cells in TILs. (C) Fractions of $CD4^+CD3^+$ T_{eff} in TILs. (D) Fractions of $CD49b^+$ NK cells in TILs. (E) Fractions of $CD44^{hi}CD62L^{lo}$ effector memory cells in $CD8^+$ TILs. (F) Fractions of $CD4^+CD25^+Foxp3^+$ T_{reg} cells in $CD4^+$ TILs. (G) Ratio of $CD8^+$ T_{eff} cells to T_{reg} cells. (H) Ratio of $CD8^+CD44^+$ T cells to T_{reg} cells. (I) Ratio of $CD8^+$ T_{eff} cells to MDSCs. (J) Fractions of $F4/80^+$ macrophages in TILs. (K) Fractions of $CD11c^+$ dendritic cells (DCs) in tumor-draining lymph nodes (TDLNs). s.c., subcutaneous. P values were determined by means of Mann-Whitney U tests. $^*P < 0.05$, $^{**}P < 0.01$, and $^{***}P < 0.001$.n.s., not significant.

ICB and TA99 antibodies, mice that received the combination therapy showed markedly higher tumor infiltration of $CD8^+$ T_{eff} cells—including effector memory $CD8^+$ TILs—and $NK1.1^+CD3^-$ NK cells (Fig. 5, B to D, $n = 7$ to 9; numbers of cells per milligram of tumor are shown in fig. S9), a lower fraction of T_{reg} cells in total $CD4^+$ TILs (Fig. 5E; fractions of $CD4^+$ TILs in fig. S10A), and lower fractions of MDSCs (fig. S10C) and macrophages in total TILs (Fig. 5F). The elevated ratios of $CD8^+$ T_{eff} cells to $CD4^+$ T_{reg} cells, $CD8^+CD44^+$ cells to T_{reg} cells, and $CD8^+$ T_{eff} cells to MDSCs (Fig. 5, G to I) indicated that the combination therapy effectively increased the fractions of antitumor immune cells in the tumors. Moreover, the fractions of dendritic cells and $CD8^+$ effector memory cells in tumor-draining

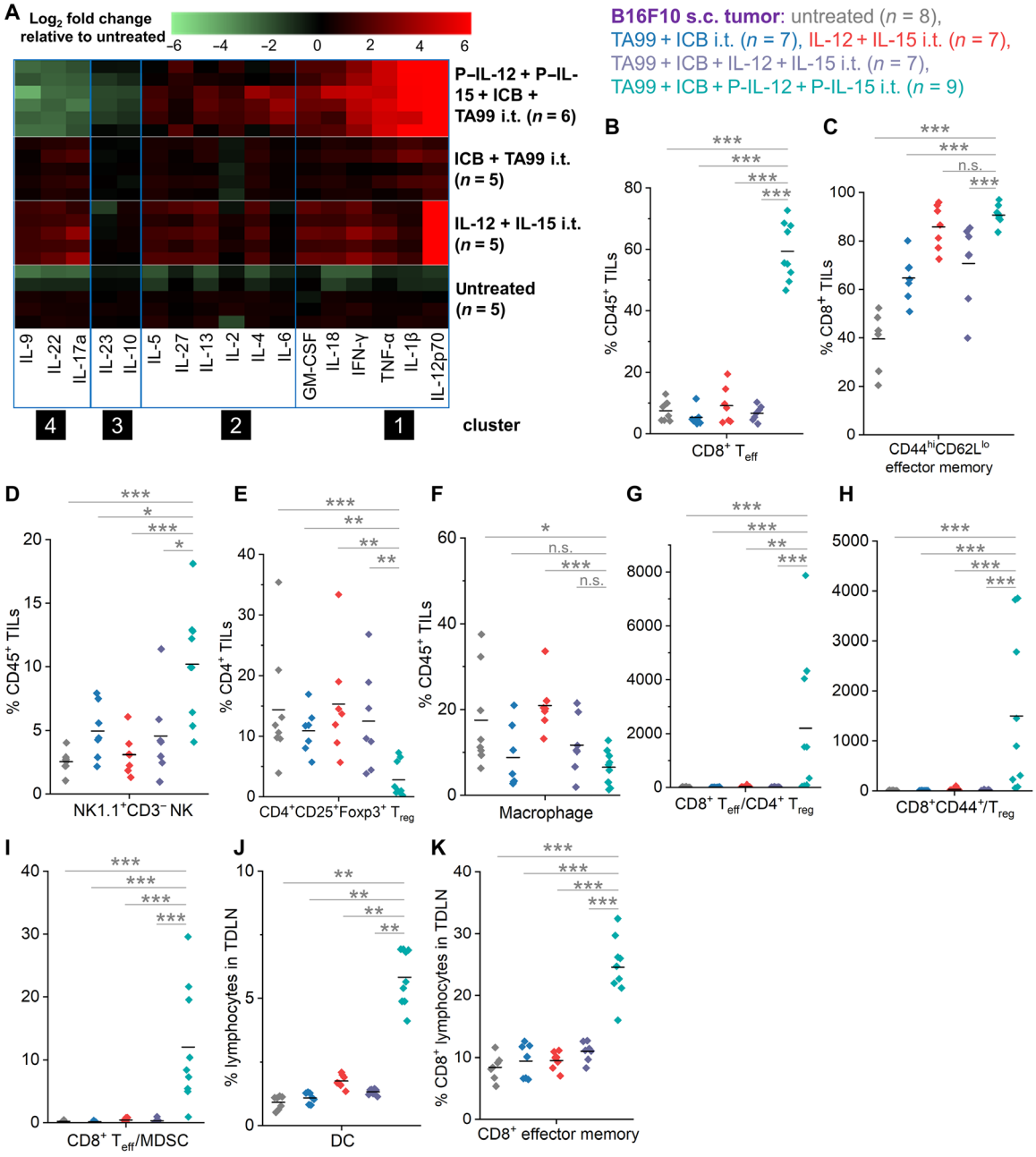

Fig. 5. Intratumoral administration of a combination of P–IL-12, P–IL-15, TA99, and ICB antibodies up-regulates inflammatory cytokines and affects immune cell infiltration in B16F10 tumors. (**A**) Luminex assay of cytokine and chemokine levels in B16F10 tumor–bearing mice treated with the indicated therapies. On day 7 following intratumoral treatment, tumors were isolated, and cytokine and chemokine levels were assayed ($n = 5$ or 6). The chemokines and cytokines were clustered by the *K*-means method. (**B** to **K**) Flow cytometry analysis of lymphocytes of untreated B16F10 tumor–bearing mice and mice that received the indicated therapies. Tumors were collected on day 7 after treatment. (B) Fractions of $CD8^+CD3^+T_{eff}$ cells in TILs. (C) Fractions of $CD44^{hi}CD62L^{lo}$ effector memory cells in $CD8^+$ TILs. (D) Fractions of $NK1.1^+CD3^-$ NK cells in TILs. (E) Fractions of $CD4^+CD25^+Foxp3^+$ T_{reg} cells in $CD4^+$ TILs. (F) Fractions of $F4/80^+$ macrophages in TILs. (G) Ratio of $CD8^+$ T_{eff} cells to T_{reg} cells. (H) Ratio of $CD8^+CD44^+$ T cells to T_{reg} cells. (I) Ratio of $CD8^+$ T_{eff} cells to MDSCs. (J) Fractions of $CD11c^+$ dendritic cells in tumor-draining lymph nodes. (K) Fractions of $CD44^{hi}CD62L^{lo}$ effector memory cells in tumor-draining lymph nodes. *P* values were determined by means of Mann-Whitney *U* tests. $^*P < 0.05$, $^{**}P < 0.01$, and $^{***}P < 0.001$.n.s., not significant.

lymph nodes were higher in the combination therapy group than in the other groups (Fig. 5, J and K). Thus, within the poorly immunogenic TMEs of B16F10 tumors, intratumoral administration of the combination therapy elicited substantial antitumor immunity that boosted early tumor regression and prolonged survival (Fig. 3H).

Local administration of combination therapy including particle-anchored cytokines reinvigorates CD8$^+$ TILs

In a previous study, we showed that B16F10 melanomas respond only partially to sustained local delivery of ICB antibodies (*55*). Recent studies have shown that T cell exhaustion and impaired production of antitumor cytokines contribute to tumor resistance to ICB immunotherapies (*1*). Data obtained in the current study (Figs. 3F and 4) led us to hypothesize that locally administered particle-anchored cytokines could reinvigorate CD8$^+$ TILs and thereby overcome ICB resistance in B16F10 tumors. To examine the proliferation and functionality of CD8$^+$ TILs in B16F10 tumors, we performed ex vivo stimulation of isolated CD8$^+$ T cells to analyze the intracellular levels of cytokines. We found that locally administered combination therapy consisting of P–IL-12, P–IL-15, TA99, and ICB antibodies resulted in a higher fraction of ki-67$^+$ cells (indicative of proliferation) in CD8$^+$ TILs than in the untreated group and groups treated with free cytokines or with ICB antibodies and TA99 (Fig. 6A). Moreover, compared with the other three groups, the combination therapy group showed higher fractions of cells that were both ki-67$^+$ (indicative of proliferation) and IFN-γ$^+$, TNF-α$^+$, and granzyme B$^+$ (indicative of cytotoxicity) (Fig. 6, B to D). Notably, we observed that most of the IFN-γ–producing CD8$^+$ TILs in the combination therapy group were also positive for TNF-α production with proliferation (Fig. 6E), indicating that the combination therapy augmented polyfunctionality in CD8$^+$ TILs.

In addition to assessing the effects of the combination therapy on TIL function, we also examined its effects on CD8$^+$ T cell states. We found that compared with CD8$^+$ TILs in untreated mice, CD8$^+$ TILs in mice that received the combination therapy showed lower fractions of inhibitory checkpoint receptors (PD-1$^+$TIM-3$^+$, PD-1$^+$TIGIT$^+$, and PD-1$^+$LAG-3$^+$) that are associated with dysfunctional T cells (Fig. 6, F to H) (*69*). The fractions of coinhibitory checkpoint receptors in the free IL-12 and IL-15 group and the TA99 and ICB antibody group were not significantly lower than the fractions in the combination therapy group. Consistently, examination of CD8$^+$ TIL subsets revealed that mice that received the combination therapy had a higher fraction of progenitor exhausted CD8$^+$ TILs (PD-1$^+$CD44$^+$Slamf6$^+$ Tim-3$^-$) and a lower fraction of terminally exhausted CD8$^+$ TILs (PD-1$^+$CD44$^+$Slamf6$^-$Tim-3$^+$) than the other groups (Fig. 6, I to K). Notably, T cell exhaustion is an important physiological adaptation to continuous antigen stimulation in cancer and contributes to tumor persistence (*69*). Progenitor, or stem-like, exhausted CD8$^+$ T cells can self-renew and respond to ICB immunotherapies, but terminally exhausted CD8$^+$ TILs cannot (*70*). Together, our results suggested that the locally administered particle-anchored cytokines rejuvenated exhausted TILs by increasing the fraction of progenitor exhausted CD8$^+$ TILs while reducing the fraction of terminally exhausted CD8$^+$ TILs and by increasing the functionality and proliferation of CD8$^+$ TILs. Therefore, our combination therapy not only safely increased the number of CD8$^+$ TILs in the TME (Fig. 5B) but also restored the polyfunctionality of CD8$^+$ TILs while reducing expression of inhibitory checkpoint receptors, thereby contributing to the observed antitumor efficacy of the combination therapy (Fig. 3H).

Local administration of the combination therapy shows potent antitumor efficacy in genetically engineered mouse models

The histology of transplanted tumors does not closely recapitulate the histology of human tumors. Therefore, we assessed the efficacy of our locally administered combination therapy in genetically engineered mouse models. We first tested female FVB/N-Tg(MMTV-PyVT)634Mul/J mice (also known as MMTV-PyMT mice), which spontaneously develop highly invasive breast ductal carcinomas in all mammary fat pads and show a high frequency of lung metastases (*71*). When the volume of the first tumor reached 50 to 100 mm^3 (usually by 8 weeks of age), we started intratumoral administration of a combination of P–IL-12 (2 μg of IL-12 per dose) every 6 days, P–IL-15 (2 μg of IL-15 per dose) every 6 days, and ICB antibodies (anti–CTLA-4 and anti–PD-1, each at 50 μg per dose) every 3 days (schedules are shown in Fig. 7A). The mice that received the combination therapy had significantly longer survival than mice that received IL-12 or ICB antibodies alone or a combination of P–IL-12 and ICB antibodies (Fig. 7A, $P = 0.00007$, 0.0004, and 0.0328, respectively, by log-rank test; $n = 4$ to 8), and they also had lower total tumor burdens (representative images are shown in Fig. 7B). Notably, the combination regimen elicited a systemic response that restrained tumor growth in distal mammary fat pads (representative images are shown in Fig. 7B).

We next used the genetically engineered mouse model *Braf*^{V600E}/*Pten*$^{-/-}$ (hereafter, these referred to as *Braf/Pten*) to examine the efficacy of our combination therapy (schedules are shown in Fig. 7C). In this model, 10 days after topical application of 4-hydroxytamoxifen to induce the expression of oncogenic *Braf*^{V600E} and deletion of tumor suppressor gene *Pten* in melanocytes, malignant melanomas form in 3 weeks (representative images are shown in Fig. 7D), and masses with pigmented areas of >150 mm^2 develop in 5 weeks (Fig. 7E). A previous study showed that ICB antibodies (anti–CTLA-4 and anti–PD-1) only slightly slow the growth of these tumors (*72*). In contrast, we found that intratumoral administration of a combination of P–IL-12, P–IL-15, and ICB antibodies starting 10 days after the first application of 4-hydroxytamoxifen (at the doses described above for MMTV-PyMT mice; schedule are shown in Fig. 7C) significantly slowed tumor growth and delayed the onset of tumor development and the median survival time was 58 days, as opposed to 43 days for the untreated mice (Fig. 7, C to E, $P = 0.0004$ by log-rank test, $n =$ 5 and 7). These results affirmed our finding that the combination of particle-anchored cytokines with ICB antibodies exhibits potent antitumor effects in difficult-to-treat genetically engineered mouse models.

DISCUSSION

The potent antitumor activities of inflammatory cytokines—including IL-12 and IL-15, which were used in this study—have motivated various strategies for their delivery to and retention in tumors (*73*). Here, we demonstrated that noncovalent anchoring of Fc-fused cytokines to intratumoral-administered PS particle surfaces can initiate antitumor immunity in immune-excluded tumors, increase infiltration of both innate and adaptive immune cells (Figs. 4 and 5), and produce robust systemic antitumor responses without systemic toxicity (Fig. 3). Rechallenge studies in a 4T1 breast tumor model (Fig. 3, D to G) demonstrated that our combination therapy generated durable

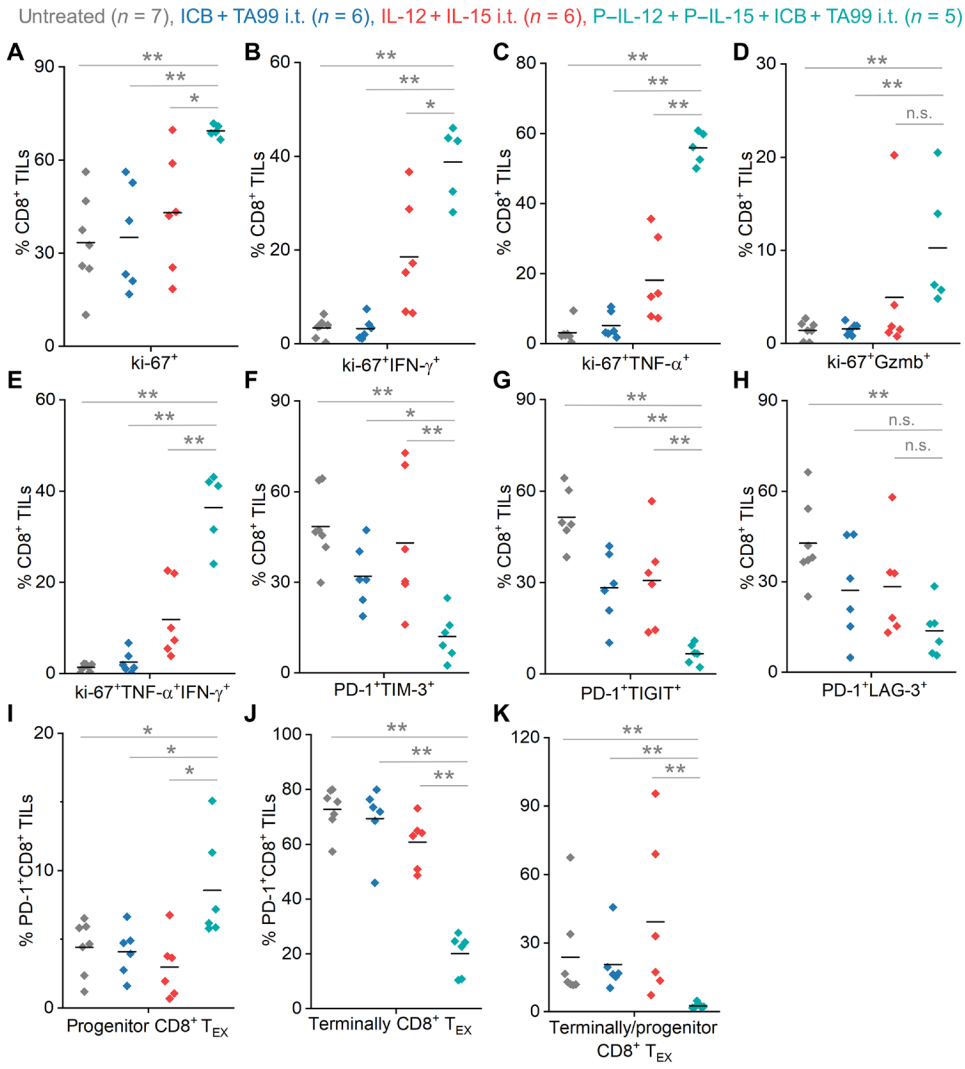

Fig. 6. Intratumoral administration of the combination therapy affects the proportions of CD8$^+$ TIL subsets and their functionality. Flow cytometry analysis of B16F10 tumor–bearing C57BL/6 mice on day 7 after administration of various therapies. (**A**) Fractions of proliferative cells (ki-67$^+$) in CD8$^+$ TILs. (**B** to **E**) Fractions of proliferative ki-67$^+$IFN-γ$^+$ (B), ki-67$^+$TNF-α$^+$ (C), ki-67$^+$Gzmb$^+$ (D), and polyfunctional ki-67$^+$TNF-α$^+$IFN-γ (E) cells in isolated CD8$^+$ TILs after ex vivo stimulation. Gzmb, granzyme B. (**F** to **H**) Fractions of CD8$^+$ TILs expressing multiple immune checkpoint molecules: (F) PD-1$^+$TIM-3$^+$CD8$^+$ TILs, (G) PD-1$^+$TIGIT$^+$CD8$^+$ TILs, and (H) PD-1$^+$LAG-3$^+$CD8$^+$ TILs. (**I** and **J**) Fractions of progenitor (I) and terminally (J) exhausted CD8$^+$ TILs (CD8$^+$ T_{EX}). (**K**) Ratios between terminally and progenitor exhausted CD8$^+$ TILs. *P* values were determined by means of Mann-Whitney *U* tests. **P* < 0.05, ***P* < 0.01. n.s., not significant.

antitumor immune memory to control disseminated metastases. Note that the syngeneic murine tumor models studied here (4T1 and B16F10) were selected because of their resistance to ICB antibody treatment. In addition, the potent combination of the particle-anchored cytokines and ICB antibodies safely improved overall survival in two transgenic tumor models (Fig. 7).

The advent of endoscopy and laparoscopic surgery procedures to access lesions (*74*) has inspired researchers to develop local immunotherapies that can be used to treat unresectable tumors or can be used as a postsurgical adjuvant that generates systemic immunities to prevent recurrence (*75*, *76*). Two local immunotherapies have been approved by the U.S. Food and Drug Administration for cancer treatment, and various dose-limiting protein therapeutics are in clinical trials as intratumoral immunotherapies, including ICB antibodies (NCT03058289), IL-12–encoding mRNA (NCT03946800), and tumor-targeted IL-2 and TNF-α (NCT04362722) (*74*). Nevertheless, there is no fundamental framework for designing optimal intratumoral delivery agents that maximize tumor retention of these potent therapeutics and minimize their systemic exposure. For many immunotherapeutics, including cytokines, the local concentration must remain within the therapeutic window long enough to allow productive engagement with desired immune cells, thereby transforming immune-excluded tumors to tumors with an inflammatory milieu in the TME. In addition, unlike conventional chemotherapeutics that must undergo cellular internalization, cytokines do not have to be taken up by cells because they function by engaging with receptors on the surface of immune cells. In this study, we showed that tumor retention of particle-anchored cytokines is particle size dependent (Fig. 2, A to D) and that intratumoral administration of microparticles prolongs the presence of cytokines in tumors. Recent work involving intratumoral injection of phosphorylated IL-12 anchored to large aluminum hydroxide particles supports our findings in this

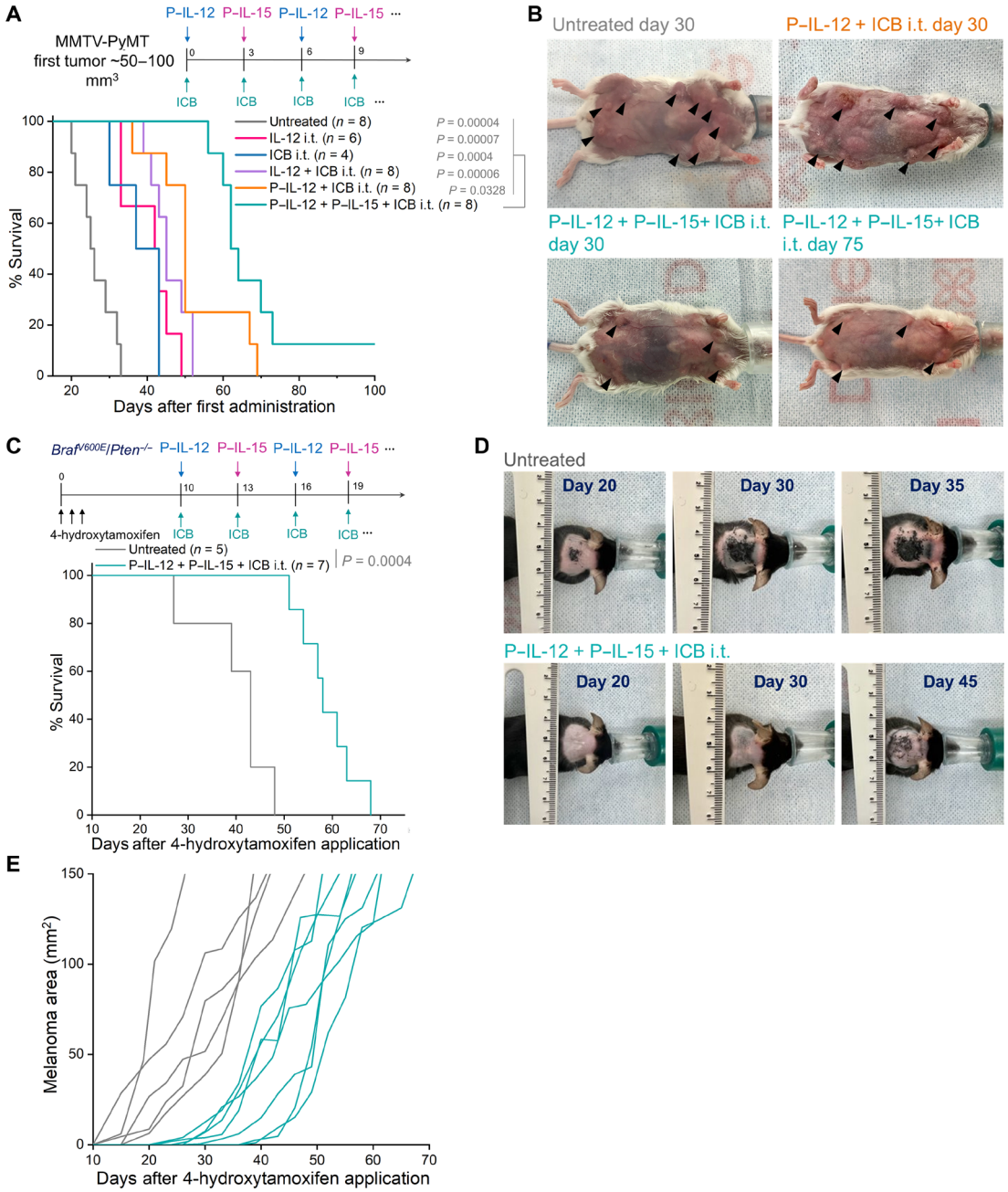

Fig. 7. Local administration of the combination of P–IL-12, P–IL-15, and ICB antibodies controls tumor growth in MMTV-PyMT and *Braf*^{V600E}/*Pten*$^{-/-}$ transgenic mice. (**A**) Overall survival of MMTV-PyMT mice that received the indicated treatments starting at 8 weeks of age (day 0). (**B**) Representative images of an untreated MMTV-PyMT mouse on day 30 (top left), a mouse that received intratumoral P–IL-12 (q6d) and ICB antibodies (q3d) on day 30 (top right), and a mouse that received P–IL-12 + P–IL-15 + ICB antibodies on day 30 (bottom left) and day 75 (bottom right). Breast tumors are indicated by black arrowheads. (**C**) Overall survival of untreated *Braf*^{V600E}/*Pten*$^{-/-}$ mice and mice that received intratumoral combination therapy. For more information, see "Subcutaneous tumor inoculation" in the Materials and methods. (**D**) Representative images of pigmented melanomas in mice from the groups in (C). (**E**) Temporal dependence of melanoma areas in mice in (C). *P* values in survival studies were compared by log-rank test.

study (*29*). Our study is also consistent with previous reports showing brief tumor retention, usually ~1 to 2 days, of intratumoral administered nanoparticles of <200 nm in size. Given the readily accessibility of Fc cytokines, our formulation provides a simple, general strategy for delivering potent immunostimulatory cytokines to induce durable antitumor immunity with minimal systemic toxicity.

One major factor in resistance to checkpoint inhibitors is the lack of tumor-infiltrating immune cells such as T cells and NK cells in tumors. In this study, we demonstrated that the prolonged presence of IL-12 and IL-15 in tumors induced a robust influx of both CD8^{+} T cells (Figs. 4B and 5B) and NK cells (Figs. 4D and 5D), in addition to increasing the fraction of dendritic cells in tumor-draining lymph

nodes (Figs. 4K and 5J). Our findings agree with the results of recent clinical studies (NCT02493361 and NCT03946800) involving the use of intratumoral IL-12–encoding mRNA and ICB antibodies, which can increase the frequency of $CD8^+$ TILs in patients who show a partial response to PD-1 blockade or have stable disease (*77*, *78*).

Moreover, we found that decreased production of inhibitory checkpoint receptors—including TIM-3, LAG-3, and TIGIT—and a reduced ratio between terminally and progenitor exhausted $CD8^+$ cells contributed to improved proliferation and polyfunctionality of $CD8^+$ TILs in mice that received the combination therapy. Our results suggest that IL-12 and IL-15 signaling could help reinvigorate exhausted $CD8^+$ T cells toward ICB antibody–responsive states, thereby generating durable antitumor immunity and immune memory. This finding agrees with the results of recent studies indicating that human $CD8^+$ TILs that are unresponsive to PD-1 blockade can be reinvigorated by IL-12 (*79*) and IL-15 (*80*).

One shortcoming of our study is that we used nondegradable PS particles to anchor the cytokines because our initial focus was to elucidate the effect of particle size on tumor retention. Nevertheless, we did not observe any toxicity, presumably because of the limited amount of PS per injection (~0.02 mg). Future studies will focus on using benign particles such as large liposomes. Nevertheless, given the generality of our formulation method, many other particulate formulations, e.g., stimulus-responsive particles, mRNA-delivery particles, and imaging modalities, could easily be adapted into our system. Collectively, our results indicate that our formulation strategy provides a platform that is likely to be amenable to many potent cytokines and protein therapeutics, which can safely orchestrate adequate immune attacks on solid tumors to improve the clinical management of cancers.

MATERIALS AND METHODS

Formulation of PS-FcBP

FcBP (sequence: GGGGSHWRGWV; Peptide 2.0, Chantilly, VA) was dissolved in 1× PBS (1 mg/ml). Carboxy-modified PS microparticle (50 mg in 5 ml of deionized water, diameter = 1 μm, zeta potential = −56 mV [equal to ~17 μmol of carboxylate per gram of particle, determined by the literature method (*45*); Polysciences or Sigma-Aldrich) was first activated using EDC (8.5 μmol; Sigma-Aldrich) and NHS (17 μmol; Sigma-Aldrich) for 15 min at room temperature. FcBP in 1× PBS solution (5 ml) was then added into the particle solution, and the reaction was stirred for overnight. The resulting PS-FcBP conjugate was washed three times using 1× PBS by the centrifuge (8000 rpm for 5 min every time), and the supernatant was discarded. The pellet was then resuspended in 1× PBS at the concentration of 20 mg/ml, and the solution was stored at 4°C.

Synthesis of Fc-Cy7 conjugate

Fifty micrograms of mouse Fc (immunoglobulin G1–mFc, ~32 kDa; SinoBiological, catalog no. 10690-MNAH) was dissolved in 0.5 ml PBS (1×). Sulfo-Cy7-NHS ester (0.15 μmol; Lumiprobe) and EDC (0.15 μmol; Sigma-Aldrich) were added into the mFc solution and were stirred at 4°C for overnight. The conjugate was purified by dialysis using 10-kDa molecular weight cutoff membrane (Spectra/Por) for 48 hours. The whole process was performed in the dark to avoid photobleach.

Formulation of PS-FcBP/Fc-Cy7 and measurement of the Fc loading efficiency

One milliliter of Fc-Cy7 (55 μg/ml in 1× PBS) was mixed with 1 ml of PS-FcBP solution (1 mg/ml), and the mixture was incubated at room temperature for 6 hours. The resulted PS-FcBP/Fc-Cy7 was washed three times using 1× PBS by the centrifuge (8000 rpm for 5 min each time), and the supernatant was removed from the particle. The obtained particles were resuspended in PBS. The supernatant and PS-FcBP/Fc-Cy7 particle solution were imaged using LI-COR Biosciences Odyssey Infrared Imaging System with the emission wavelength at 800 nm (for Cy7).

Formulation of P–IL-12 and P–IL-15

Fc–IL-12 (SinoBiological, catalog no. CT021-M02H) was mixed with PS-FcBP in 1× PBS at the Fc–IL-12/PS-FcBP ratio of 1:10 (w/w) and was incubated for overnight at 4°C (or for 6 hours at room temperature). The formulated P–IL-12 was then washed three times using 1× PBS by the centrifuge (8000 rpm for 5 min each time) and was stored at 4°C. P–IL-15 was formulated using Fc-IL-15 (Acro Biosystems, catalog no. IL5-M5255) following the same protocol as P–IL-12.

Animal studies

All animal work was conducted in appliance to the National Institutes of Health Guide for the Care and Use of Laboratory Animals under protocols approved by Virginia Tech Institutional Animal Care and Use Committee and Institutional Biosafety Committee.

Mice and cell lines

Balb/c and C57BL/6 mice (ages 6 to 8 weeks female from the Jackson Laboratory or Envigo), MMTV-PyMT male (ages 4 to 6 weeks from the Jackson Laboratory, JAX stock #002374), FVB/NJ females mice (ages 4 to 6 weeks from the Jackson Laboratory, JAX stock #001800), and B6.Cg-Tg(Tyr-cre/ERT2)13Bos $Braf^{tm1Mmcm}$ $Ptent^{m1Hwu}$/BosJ breeding pairs (ages 4 to 6 weeks from the Jackson Laboratory, JAX stock #013590) were used and maintained following the animal protocol. MMTV-PyMT female mice with spontaneously developed breast cancer (6 to 7 weeks age) were crossed of MMTV-PyMT male and FVB/NJ females mice, and genotyped (Transnetyx). Tyr:Cre-ER^+/LSL-$Braf^{V600E}$/$Pten^{fl/fl}$ mice (designated as $Braf^{V600E}$/$Pten^{fl/fl}$) with inducible melanoma tumors were generated by male [hemizygous for Tg(Tyr-cre/ERT2)13Bos, homozygous for $Braf^{tm1Mmcm}$, and homozygous for $Pten^{tm1Hwu}$] and female [noncarrier for Tg(Tyr-cre/ERT2)13Bos, heterozygous for $Braf^{tm1Mmcm}$, and homozygous for $Pten^{tm1Hwu}$] and genotyped (Transnetyx). The mice of hemizygous for Tg(Tyr-cre/ERT2)13Bos, heterozygous for $Braf^{tm1Mmcm}$, and homozygous for $Pten^{tm1Hwu}$ (age, ~8 weeks) were used for tumor induction. All mice were group-housed (five mice per cage) and maintained under a regular light-dark cycle altered every 12 hours with free access to water and food under pathogen-free conditions in a barrier facility in Virginia Tech. Murine breast cancer 4T1 and murine melanoma B16F10 cell lines were originally purchased from American Type Culture Collection (Manassas, VA). All cells were maintained at 37°C with 5% CO_2 in culture medium according to the instructions, supplemented with 10% heat-inactivated FBS and penicillin/streptomycin (all from Life Technology, Grand Island, NY). All cells were tested to be free of mycoplasma.

Subcutaneous tumor inoculation

For subcutaneous inoculation of single B16F10 and 4T1 tumors, 5×10^5 cells in 50 μl of sterile PBS (1×) were subcutaneously injected into the shaved nape area of C57BL/6 or balb/c female mice. Treatments were started when 4T1 tumors reached ~50 to 100 mm^3 or 7 days after B16F10 tumor inoculation. The body weight and tumor size were measured every 2 to 3 days after the treatment started. Tumor length and width were measured with a digital caliper, and the tumor volume was calculated using the following equation: tumor volume = length × width × width / 2. Mice were euthanized when their tumor volumes reached a predetermined end point (1000 mm^3) or when their body weights dropped over 10 to 15%. For tumor rechallenge studies, mice that overcame tumors were inoculated with the same amount of tumor cells (5×10^5 cells) in the right flank and monitored for another 4 weeks. For evaluation of antimetastatic effect, mice that had been cured by the combination regimen were intravenously injected with 5×10^5 4T1 tumor cells via tail-vein injection and monitored for another 4 weeks.

Whole-body fluorescence imaging of mice

The balb/c mice were firstly shaved and subcutaneously inoculated with 5×10^5 4T1 cells in 50 μl PBS (1×) on the back of the neck after the hair was removed. The balb/c mice were fed with alfalfa-free food for at least 1 week before the study to minimize the gastrointestinal background autofluorescence. Once the tumor reached ~50 mm^3, a PS-FcBP/Fc-Cy7 (50 μg/ml) in 20 μl of sterile PBS solution (1×) was intratumorally injected into the 4T1 tumor. Whole-body fluorescence imaging of mice was performed with LI-COR Biosciences Odyssey Infrared Imaging System with emission wavelength at 700 nm (for autofluorescence in mice body) and 800 nm (for Fc-Cy7) at designated time points. Tumors were explanted at 168 hours and imaged to get the fluorescence intensity. The analysis of the results was carried out using Origin software (Northampton, MA) by fitting the normalized fluorescence intensity (I)–time (t) curve into an exponential decay model according to Eq. 1.

$$I = a \cdot \exp(t / T1) + b \quad (1)$$

where a, b, and $T1$ are all constants fitted by Origin software. The starting point for the curve fitting was the peak value of the normalized fluorescence intensity, usually at 6 or 24 hours. The obtained $T1$ value was used to calculate the decay half-life τ based on Eq. 2.

$$\tau = \ln(2) \cdot T1 \quad (2)$$

Note that the fluorescence intensity at $t = 0$ was normalized as 1.

Subcutaneous tumor treatment

Intratumoral treatments into the subcutaneous tumors were administered in 30 μl of sterile PBS. Intraperitoneal treatments were administered in 100 μl of sterile PBS (1×). In total, 50 μg of anti–CTLA-4 (clone 9H10, BioXCell, Lebanon, NH, catalog no. BP0131) and anti–PD-1 (clone RMP1-14, BioXCell, catalog no. BE0146), 100 μg of TA99 (or anti-TYRP-1, BioXCell, catalog no. BE0151), 2 μg of Fc–IL-12 (SinoBiological, catalog no. CT021-M02H), 2 μg of Fc–IL-15 (ACROBiosystems, catalog no. IL5-M5255), and equivalent P–IL-12 and P–IL-15 were administered each per dose. All mice were treated under anesthesia. Detailed dose and schedule of the cytokines and antibodies are described in Figs. 3H and 7A for different tumor models.

Induction and treatment of *Braf*^{V600E}/*Pten*$^{fl/fl}$ autochthonous melanoma

On day 0, 6- to 8-week-old *Braf*^{V600E}/*Pten*$^{fl/fl}$ mice were painted with 5 μl of ethanol solution of 4-hydroxytamoxifen (Sigma-Aldrich) at 5 mg/ml on the shaved nape of the mice for three consecutive days. On day 10, mice were intratumorally treated with P–IL-12 (equivalent of 2 μg of IL-12, q6d), P–IL-15 (equivalent of 2 μg of IL-15, q6d), 100 μg of TA99 (q3d), 50 μg of anti–CTLA-4 (clone 9H10, BioXCell, q3d), and 50 μg of anti–PD-1 (clone 29F.1A12, BioXCell, q3d) in 50 μl of sterile PBS (1×) following the dose schedule described in Fig. 7C. Tumor size was measured as surface area, which was taken photos with a caliper and quantified by Fiji ImageJ analysis software. Mice were euthanized when tumors areas exceeded 150 mm^2.

Flow cytometry analysis of tumor lymphocytes

Tumors and lymph nodes were resected from mice, weighted, and gently ground to generate single-cell suspensions through a 70-μm cell strainer. Red blood cells were lysed with RBC lysis buffer (BioLegend, San Diego, CA). Cells were counted and resuspended in cell staining buffer (BioLegend) and used for flow cytometry staining. Nonspecific immunofluorescence staining was prevented by incubating cells with TruStain fcX (anti-mouse CD16/32) (clone 93, BioLegend) antibody in 100 μl of volume for ~10 min on ice. Cell surface staining with antibody was performed according to the manufacturer's instructions (BioLegend) with a dilution ratio of 1:100. Fluorescent antibodies (all from BioLegend) used included CD45 (clone 30-F11), CD3 (clone 17A2), CTLA-4 (CD152, clone UC10-4B9), CD11c (clone N418), CD49b (clone HMα2), PD-1 (CD279, clone RMP1-30), F4/80 (clone BM8), CD19 (clone 6D5), CD4 (clone GK1.5), Ly-6G (clone 1A8), CD11b (clone M1/70), CD25 (clone PC61), CD8a (clone 53-6.7), CD44 (clone IM7), CD62L (clone MEL-14), Ly-6C (clone HK1.4), NK1.1 (CD161, clone PK136), TIM-3 (CD366, clone RMT3-23 for C57BL/6 mice, and clone B8.2C12 for balb/c mice), LAG-3 (CD223, clone C9B7W), Slamf6 (Ly-108, clone 330-AJ), IFN-γ (clone XMG1.2), TNF-α (clone MP6-XT22), granzyme B (clone QA16A02), ki-67 (clone 16A8), and Foxp3 (clone MF-14). Fixable live/dead cell discrimination was performed using Zombie Aqua Fixable Viability Kit according to the manufacturer's protocol (BioLegend). For intracellular staining, cells were fixed and permeabilized with the True-Nuclear Transcription Factor Staining Kit (BioLegend) following the manufacturer's instructions before being stained with antibodies. All flow cytometry data collection was performed using BD FACSAria flow cytometer (BD Biosciences, San Jose, CA) and analyzed using FlowJo software (Ashland, OR).

$CD8^+$ T cell activation and cytokine analysis

Tumors were resected from mice, weighted, and gently ground to generate single-cell suspensions through a 70-μm cell strainer. Cells were counted and resuspended in cell culture medium and plated at a density around 1×10^6 cells per well in a 24-well plate. The suspension was incubated with cell activation cocktail (containing brefeldin A, phorbol 12-myristate 13-acetate, and ionomycin; BioLegend) for 6 hours at 37°C with 5% CO_2 following the manufacturer's instructions, followed by surface and intracellular

flow cytometry staining to detect IFN-γ, TNF-α, other cytokines, and cell markers.

Luminex analysis of cytokine/chemokine

For cytokine/chemokine analysis of serum and tumor lysate, blood was collected at 1, 24, and 72 hours after treatment, while tumors were collected and homogenized using Branson SFX150 Sonifier in cell lysis buffer (Thermo Fisher Scientific, catalog no. EPX-99999-000) with 1% halt protease and phosphatase inhibitors (Thermo Fisher Scientific, catalog no. 78442). The lysates were incubated with tissue at 4°C for 30 min with rotation and then centrifuged at 16,000*g* to remove debris. Lysates were aliquoted and stored at −80°C until analysis. Samples were assayed using a Luminex bead-based enzyme-linked immunosorbent assay (Thermo Fisher Scientific Cytokine & Chemokine Convenience 36-Plex Mouse ProcartaPlex Panel 1A, catalog number: EPXR360-26092-901, $T_H1/T_H2/T_H9/T_H17/T_H22/T_{reg}$ Cytokine 17-Plex Mouse ProcartaPlex Panel, catalog no. EPX170-26087-901, and Mouse ProcartaPlex Mix&Match 12-plex, catalog no. PPX-12-MXYMMCJ) following the manufacturer's instructions.

Histology

For hematoxylin and eosin staining, balb/c mice were euthanized 5 days after the first treatment, while C57BL/6 mice were euthanized 14 days after the first treatment. The lung, liver, heart, spleen, kidney, and tumors were fixed in 10% formalin, embedded in paraffin, and stained with hematoxylin and eosin. The images were acquired under identical acquisition settings and subsequently processed using Fiji ImageJ analysis software.

Statistical analysis

Statistical analysis was performed using Origin software (Northampton, MA). Most comparisons between groups were assessed using Mann-Whitney *U* test (two-sided). Kaplan-Meier survival curves were compared using log-rank test. The *n* values and specific statistical methods are indicated in figure legends.

Supplementary Materials

This PDF file includes:

Figs. S1 to S12

REFERENCES AND NOTES

1. A. Kalbasi, A. Ribas, Tumour-intrinsic resistance to immune checkpoint blockade. *Nat. Rev. Immunol.* **20**, 25–39 (2020).
2. S. C. Wei, J. H. Levine, A. P. Cogdill, Y. Zhao, N.-A. A. S. Anang, M. C. Andrews, P. Sharma, J. Wang, J. A. Wargo, D. Pe'er, J. P. Allison, Distinct cellular mechanisms underlie anti-CTLA-4 and anti-PD-1 checkpoint blockade. *Cell* **170**, 1120–1133.e17 (2017).
3. K. D. Moynihan, C. F. Opel, G. L. Szeto, A. Tzeng, E. F. Zhu, J. M. Engreitz, R. T. Williams, K. Rakhra, M. H. Zhang, A. M. Rothschilds, S. Kumari, R. L. Kelly, B. H. Kwan, W. Abraham, K. Hu, N. K. Mehta, M. J. Kauke, H. Suh, J. R. Cochran, D. A. Lauffenburger, K. D. Wittrup, D. J. Irvine, Eradication of large established tumors in mice by combination immunotherapy that engages innate and adaptive immune responses. *Nat. Med.* **22**, 1402–1410 (2016).
4. I. Vitale, E. Shema, S. Loi, L. Galluzzi, Intratumoral heterogeneity in cancer progression and response to immunotherapy. *Nat. Med.* **27**, 212–224 (2021).
5. D. Briukhovetska, J. Dörr, S. Endres, P. Libby, C. A. Dinarello, S. Kobold, Interleukins in cancer: From biology to therapy. *Nat. Rev. Cancer* **21**, 481–499 (2021).
6. P. G. Holder, S. A. Lim, C. S. Huang, P. Sharma, Y. S. Dagdas, B. Bulutoglu, J. T. Sockolosky, Engineering interferons and interleukins for cancer immunotherapy. *Adv. Drug Deliv. Rev.* **182**, 114112 (2022).
7. P. Berraondo, M. F. Sanmamed, M. C. Ochoa, I. Etxeberria, M. A. Aznar, J. L. Pérez-Gracia, M. E. Rodríguez-Ruiz, M. Ponz-Sarvise, E. Castañón, I. Melero, Cytokines in clinical cancer immunotherapy. *Br. J. Cancer* **120**, 6–15 (2019).
8. J. R. Quesada, J. Reuben, J. T. Manning, E. M. Hersh, J. U. Gutterman, Alpha interferon for induction of remission in hairy-cell leukemia. *N. Engl. J. Med.* **310**, 15–18 (1984).
9. S. A. Rosenberg, M. T. Lotze, L. M. Muul, S. Leitman, A. E. Chang, S. E. Ettinghausen, Y. L. Matory, J. M. Skibber, E. Shiloni, J. T. Vetto, C. A. Seipp, C. Simpson, C. M. Reichert, Observations on the systemic administration of autologous lymphokine-activated killer cells and recombinant interleukin-2 to patients with metastatic cancer. *N. Engl. J. Med.* **313**, 1485–1492 (1985).
10. M. B. Atkins, M. T. Lotze, J. P. Dutcher, R. I. Fisher, G. Weiss, K. Margolin, J. Abrams, M. Sznol, D. Parkinson, M. Hawkins, C. Paradise, L. Kunkel, S. A. Rosenberg, High-dose recombinant interleukin 2 therapy for patients with metastatic melanoma: Analysis of 270 patients treated between 1985 and 1993. *J. Clin. Oncol.* **17**, 2105–2116 (1999).
11. G. I. Kirchner, A. Franzke, J. Buer, W. Beil, M. Probst-Kepper, F. Wittke, K. Overmann, S. Lassmann, R. Hoffmann, H. Kirchner, A. Ganser, J. Atzpodien, Pharmacokinetics of recombinant human interleukin-2 in advanced renal cell carcinoma patients following subcutaneous application. *Br. J. Clin. Pharmacol.* **46**, 5–10 (1998).
12. J. P. Leonard, M. L. Sherman, G. L. Fisher, L. J. Buchanan, G. Larsen, M. B. Atkins, J. A. Sosman, J. P. Dutcher, N. J. Vogelzang, J. L. Ryan, Effects of single-dose interleukin-12 exposure on interleukin-12-associated toxicity and interferon-gamma production. *Blood* **90**, 2541–2548 (1997).
13. M. B. Atkins, M. J. Robertson, M. Gordon, M. T. Lotze, M. DeCoste, J. S. DuBois, J. Ritz, A. B. Sandler, H. D. Edington, P. D. Garzone, J. W. Mier, C. M. Canning, L. Battiato, H. Tahara, M. L. Sherman, Phase I evaluation of intravenous recombinant human interleukin 12 in patients with advanced malignancies. *Clin. Cancer Res.* **3**, 409–417 (1997).
14. D. Lowe, "Nektar reads out. Unfortunately," *Science* (2022); www.science.org/content/blog-post/nektar-reads-out-unfortunately.
15. C. M. van Herpen, R. Huijbens, M. Looman, J. de Vries, H. Marres, J. Van De Ven, R. Hermsen, G. J. Adema, P. H. De Mulder, Pharmacokinetics and immunological aspects of a phase Ib study with intratumoral administration of recombinant human interleukin-12 in patients with head and neck squamous cell carcinoma: A decrease of T-bet in peripheral blood mononuclear cells. *Clin. Cancer Res.* **9**, 2950–2956 (2003).
16. O. Eton, M. G. Rosenblum, S. S. Legha, W. Zhang, M. Jo East, A. Bedikian, N. Papadopoulos, A. Buzaid, R. S. Benjamin, Phase I trial of subcutaneous recombinant human interleukin-2 in patients with metastatic melanoma. *Cancer* **95**, 127–134 (2002).
17. B. Kwong, S. A. Gai, J. Elkhader, K. D. Wittrup, D. J. Irvine, Localized immunotherapy via liposome-anchored anti-CD137 + IL-2 prevents lethal toxicity and elicits local and systemic antitumor immunity. *Cancer Res.* **73**, 1547–1558 (2013).
18. S. L. Hewitt, A. Bai, D. Bailey, K. Ichikawa, J. Zielinski, R. Karp, A. Apte, K. Arnold, S. J. Zacharek, M. S. Iliou, K. Bhatt, M. Garnaas, F. Musenge, A. Davis, N. Khatwani, S. V. Su, G. MacLean, S. J. Farlow, K. Burke, J. P. Frederick, Durable anticancer immunity from intratumoral administration of IL-23, IL-36γ, and OX40L mRNAs. *Sci. Transl. Med.* **11**, eaat9143 (2019).
19. J. Kim, W. A. Li, Y. Choi, S. A. Lewin, C. S. Verbeke, G. Dranoff, D. J. Mooney, Injectable, spontaneously assembling, inorganic scaffolds modulate immune cells in vivo and increase vaccine efficacy. *Nat. Biotechnol.* **33**, 64–72 (2015).
20. K. Xu, F. Lee, S. J. Gao, J. E. Chung, H. Yano, M. Kurisawa, Injectable hyaluronic acid-tyramine hydrogels incorporating interferon-α2a for liver cancer therapy. *J. Control. Release* **166**, 203–210 (2013).
21. Q. Lv, C. He, F. Quan, S. Yu, X. Chen, DOX/IL-2/IFN-γ co-loaded thermo-sensitive polypeptide hydrogel for efficient melanoma treatment. *Bioact. Mater.* **3**, 118–128 (2017).
22. X. Wu, Y. Wu, H. Ye, S. Yu, C. He, X. Chen, Interleukin-15 and cisplatin co-encapsulated thermosensitive polypeptide hydrogels for combined immuno-chemotherapy. *J. Control. Release* **255**, 81–93 (2017).
23. D. A. Zaharoff, K. W. Hance, C. J. Rogers, J. Schlom, J. W. Greiner, Intratumoral immunotherapy of established solid tumors with chitosan/IL-12. *J. Immunother.* **33**, 697–705 (2010).
24. C. G. Park, C. A. Hartl, D. Schmid, E. M. Carmona, H.-J. Kim, M. S. Goldberg, Extended release of perioperative immunotherapy prevents tumor recurrence and eliminates metastases. *Sci. Transl. Med.* **10**, eaar1916 (2018).
25. J. Hanes, A. Sills, Z. Zhao, K. W. Suh, B. Tyler, F. DiMeco, D. J. Brat, M. A. Choti, K. W. Leong, D. M. Pardoll, H. Brem, Controlled local delivery of interleukin-2 by biodegradable polymers protects animals from experimental brain tumors and liver tumors. *Pharm. Res.* **18**, 899–906 (2001).
26. J. Ishihara, K. Fukunaga, A. Ishihara, H. M. Larsson, L. Potin, P. Hosseinchi, G. Galliverti, M. A. Swartz, J. A. Hubbell, Matrix-binding checkpoint immunotherapies enhance antitumor efficacy and reduce adverse events. *Sci. Transl. Med.* **9**, eaan0401 (2017).
27. J. Ishihara, A. Ishihara, K. Sasaki, S. S.-Y. Lee, J.-M. Williford, M. Yasui, H. Abe, L. Potin, P. Hosseinchi, K. Fukunaga, M. M. Raczy, L. T. Gray, A. Mansurov, K. Katsumata, M. Fukayama, S. J. Kron, M. A. Swartz, J. A. Hubbell, Targeted antibody and cytokine cancer immunotherapies through collagen affinity. *Sci. Transl. Med.* **11**, eaau3259 (2019).
28. N. Momin, N. K. Mehta, N. R. Bennett, L. Ma, J. R. Palmeri, M. M. Chinn, E. A. Lutz, B. Kang, D. J. Irvine, S. Spranger, K. D. Wittrup, Anchoring of intratumorally administered cytokines to collagen safely potentiates systemic cancer immunotherapy. *Sci. Transl. Med.* **11**, eaaw2614 (2019).

29. Y. Agarwal, L. E. Milling, J. Y. H. Chang, L. Santollani, A. Sheen, E. A. Lutz, A. Tabet, J. Stinson, K. Ni, K. A. Rodrigues, T. J. Moyer, M. B. Melo, D. J. Irvine, K. D. Wittrup, Intratumourally injected alum-tethered cytokines elicit potent and safer local and systemic anticancer immunity. *Nat. Biomed. Eng.* **6**, 129–143 (2022).
30. A. M. Levin, D. L. Bates, A. M. Ring, C. Krieg, J. T. Lin, L. Su, I. Moraga, M. E. Raeber, G. R. Bowman, P. Novick, V. S. Pande, C. G. Fathman, O. Boyman, K. C. Garcia, Exploiting a natural conformational switch to engineer an interleukin-2 'superkine'. *Nature* **484**, 529–533 (2012).
31. D.-A. Silva, S. Yu, U. Y. Ulge, J. B. Spangler, K. M. Jude, C. Labão-Almeida, L. R. Ali, A. Quijano-Rubio, M. Ruterbusch, I. Leung, T. Biary, S. J. Crowley, E. Marcos, C. D. Walkey, B. D. Weitzner, F. Pardo-Avila, J. Castellanos, L. Carter, L. Stewart, S. R. Riddell, M. Pepper, G. J. L. Bernardes, M. Dougan, K. C. Garcia, D. Baker, De novo design of potent and selective mimics of IL-2 and IL-15. *Nature* **565**, 186–191 (2019).
32. J. T. Sockolosky, E. Trotta, G. Parisi, L. Picton, L. L. Su, A. C. Le, A. Chhabra, S. L. Silveria, B. M. George, I. C. King, M. R. Tiffany, K. Jude, L. V. Sibener, D. Baker, J. A. Shizuru, A. Ribas, J. A. Bluestone, K. C. Garcia, Selective targeting of engineered T cells using orthogonal IL-2 cytokine-receptor complexes. *Science* **359**, 1037–1042 (2018).
33. I. Moraga, J. B. Spangler, J. L. Mendoza, M. Gakovic, T. S. Wehrman, P. Krutzik, K. C. Garcia, Synthekines are surrogate cytokine and growth factor agonists that compel signaling through non-natural receptor dimers. *eLife* **6**, e22882 (2017).
34. L. A. Perdue, P. Do, C. David, A. Chyong, A. V. Kellner, A. Ruggieri, H. R. Kim, K. Salaita, G. B. Lesinski, C. C. Porter, E. C. Dreaden, Optical control of cytokine signaling via bioinspired, polymer-induced latency. *Biomacromolecules* **21**, 2635–2644 (2020).
35. E. J. Hsu, X. Cao, B. Moon, J. Bae, Z. Sun, Z. Liu, Y.-X. Fu, A cytokine receptor-masked IL2 prodrug selectively activates tumor-infiltrating lymphocytes for potent antitumor therapy. *Nat. Commun.* **12**, 2768 (2021).
36. A. Mansurov, P. Hosseinchi, K. Chang, A. L. Lauterbach, L. T. Gray, A. T. Alpar, E. Budina, A. J. Slezak, S. Kang, S. Cao, A. Solanki, S. Gomes, J.-M. Williford, M. A. Swartz, J. L. Mendoza, J. Ishihara, J. A. Hubbell, Masking the immunotoxicity of interleukin-12 by fusing it with a domain of its receptor via a tumour-protease-cleavable linker. *Nat. Biomed. Eng.* **6**, 819–829 (2022).
37. C. J. Nirschl, H. R. Brodkin, D. J. Hicklin, N. Ismail, K. Morris, C. Seidel-Dugan, P. Steiner, Z. Steuert, J. M. Sullivan, E. Tyagi, W. M. Winston, A. Salmeron, Discovery of a conditionally activated IL-2 that promotes antitumor immunity and induces tumor regression. *Cancer Immunol. Res.* **10**, 581–596 (2022).
38. G. Adams, S. Vessillier, H. Dreja, Y. Chernajovsky, Targeting cytokines to inflammation sites. *Nat. Biotechnol.* **21**, 1314–1320 (2003).
39. W. R. Strohl, D. M. Knight, Discovery and development of biopharmaceuticals: Current issues. *Curr. Opin. Biotechnol.* **20**, 668–672 (2009).
40. D. M. Czajkowsky, J. Hu, Z. Shao, R. J. Pleass, Fc-fusion proteins: New developments and future perspectives. *EMBO Mol. Med.* **4**, 1015–1028 (2012).
41. W. L. DeLano, M. H. Ultsch, A. M. de Vos, J. A. Wells, Convergent solutions to binding at a protein-protein interface. *Science* **287**, 1279–1283 (2000).
42. H. Yang, P. V. Gurgel, R. G. Carbonell, Hexamer peptide affinity resins that bind the Fc region of human immunoglobulin G. *J. Pept. Res.* **66**, 120–137 (2005).
43. H. L. Zhao, X. Q. Yao, C. Xue, Y. Wang, X. H. Xiong, Z. M. Liu, Increasing the homogeneity, stability and activity of human serum albumin and interferon-α2b fusion protein by linker engineering. *Protein Expr. Purif.* **61**, 73–77 (2008).
44. R. Tong, L. D. Yala, T. M. Fan, J. J. Cheng, The formulation of aptamer-coated paclitaxel-polylactide nanoconjugates and their targeting to cancer cells. *Biomaterials* **31**, 3043–3053 (2010).
45. S. Zhu, U. Panne, K. Rurack, A rapid method for the assessment of the surface group density of carboxylic acid-functionalized polystyrene microparticles. *Analyst* **138**, 2924–2930 (2013).
46. B. D. Chithrani, A. A. Ghazani, W. C. W. Chan, Determining the size and shape dependence of gold nanoparticle uptake into mammalian cells. *Nano Lett.* **6**, 662–668 (2006).
47. S. E. A. Gratton, P. A. Ropp, P. D. Pohlhaus, J. C. Luft, V. J. Madden, M. E. Napier, J. M. DeSimone, The effect of particle design on cellular internalization pathways. *Proc. Natl. Acad. Sci. U.S.A.* **105**, 11613–11618 (2008).
48. Y. Tabata, Y. Ikada, Effect of the size and surface charge of polymer microspheres on their phagocytosis by macrophage. *Biomaterials* **9**, 356–362 (1988).
49. J. B. Spangler, I. Moraga, J. L. Mendoza, K. C. Garcia, Insights into cytokine–Receptor interactions from cytokine engineering. *Annu. Rev. Immunol.* **33**, 139–167 (2015).
50. R. K. Jain, T. Stylianopoulos, Delivering nanomedicine to solid tumors. *Nat. Rev. Clin. Oncol.* **7**, 653–664 (2010).
51. T. Nomura, N. Koreeda, F. Yamashita, Y. Takakura, M. Hashida, Effect of particle size and charge on the disposition of lipid carriers after intratumoral injection into tissue-isolated tumors. *Pharm. Res.* **15**, 128–132 (1998).
52. Y. Li, Z. Su, W. Zhao, X. Zhang, N. Momin, C. Zhang, K. D. Wittrup, Y. Dong, D. J. Irvine, R. Weiss, Multifunctional oncolytic nanoparticles deliver self-replicating IL-12 RNA to eliminate established tumors and prime systemic immunity. *Nat. Cancer* **1**, 882–893 (2020).
53. C. Hotz, T. R. Wagenaar, F. Gieseke, D. S. Bangari, M. Callahan, H. Cao, J. Diekmann, M. Diken, C. Grunwitz, A. Hebert, K. Hsu, M. Bernardo, K. Karikó, S. Kreiter, A. N. Kuhn, M. Levit, N. Malkova, S. Masciari, J. Pollard, H. Qu, S. Ryan, A. Selmi, J. Schlereth, K. Singh, F. Sun, B. Tillmann, T. Tolstykh, W. Weber, L. Wicke, S. Witzel, Q. Yu, Y.-A. Zhang, G. Zheng, J. Lager, G. J. Nabel, U. Sahin, D. Wiederschain, Local delivery of mRNA-encoded cytokines promotes antitumor immunity and tumor eradication across multiple preclinical tumor models. *Sci. Transl. Med.* **13**, eabc7804 (2021).
54. K. G. Nguyen, M. R. Vrabel, S. M. Mantooth, J. J. Hopkins, E. S. Wagner, T. A. Gabaldon, D. A. Zaharoff, Localized interleukin-12 for cancer immunotherapy. *Front. Immunol.* **11**, 575597 (2020).
55. A. L. Chin, S. Jiang, E. Jang, L. Niu, L. Li, X. Jia, R. Tong, Implantable optical fibers for immunotherapeutics delivery and tumor impedance measurement. *Nat. Commun.* **12**, 5138 (2021).
56. A. Ghochikyan, A. Davtyan, A. Hovakimyan, H. Davtyan, A. Poghosyan, A. Bagaev, R. I. Ataullakhanov, E. L. Nelson, M. G. Agadjanyan, Primary 4T1 tumor resection provides critical "window of opportunity" for immunotherapy. *Clin. Exp. Metastasis* **31**, 185–198 (2014).
57. M. G. Lechner, S. S. Karimi, K. Barry-Holson, T. E. Angell, K. A. Murphy, C. H. Church, J. R. Ohlfest, P. Hu, A. L. Epstein, Immunogenicity of murine solid tumor models as a defining feature of in vivo behavior and response to immunotherapy. *J. Immunother.* **36**, 477–489 (2013).
58. M. O. Kilinc, K. S. Aulakh, R. E. Nair, S. A. Jones, P. Alard, M. M. Kosiewicz, N. K. Egilmez, Reversing tumor immune suppression with intratumoral IL-12: Activation of tumor-associated T effector/memory cells, induction of T suppressor apoptosis, and infiltration of $CD8^+$ T effectors. *J. Immunol.* **177**, 6962–6973 (2006).
59. J. J. Milner, H. Nguyen, K. Omilusik, M. Reina-Campos, M. Tsai, C. Toma, A. Delpoux, B. S. Boland, S. M. Hedrick, J. T. Chang, A. W. Goldrath, Delineation of a molecularly distinct terminally differentiated memory CD8 T cell population. *Proc. Natl. Acad. Sci. U.S.A.* **117**, 25667–25678 (2020).
60. W. Lasek, J. Golab, W. Maśliński, T. Switaj, E. Z. Bałkowiec, T. Stokłosa, A. Giermasz, M. Malejczyk, M. Jakóbisiak, Subtherapeutic doses of interleukin-15 augment the antitumor effect of interleukin-12 in a B16F10 melanoma model in mice. *Eur. Cytokine Netw.* **10**, 345–356 (1999).
61. E. Di Carlo, A. Comes, S. Basso, A. De Ambrosis, R. Meazza, P. Musiani, K. Moelling, A. Albini, S. Ferrini, The combined action of IL-15 and IL-12 gene transfer can induce tumor cell rejection without T and NK cell involvement. *J. Immunol.* **165**, 3111–3118 (2000).
62. P. S. Backhaus, R. Veinalde, L. Hartmann, J. E. Dunder, L. M. Jeworowski, J. Albert, B. Hoyler, T. Poth, D. Jäger, G. Ungerechts, C. E. Engeland, Immunological effects and viral gene expression determine the efficacy of oncolytic measles vaccines encoding IL-12 or IL-15 agonists. *Virus* **11**, 914 (2019).
63. J. Cany, A. B. van der Waart, J. Spanholtz, M. Tordoir, J. H. Jansen, R. van der Voort, N. M. Schaap, H. Dolstra, Combined IL-15 and IL-12 drives the generation of $CD34^+$-derived natural killer cells with superior maturation and alloreactivity potential following adoptive transfer. *Oncoimmunology* **4**, e1017701 (2015).
64. T. A. Waldmann, The biology of interleukin-2 and interleukin-15: Implications for cancer therapy and vaccine design. *Nat. Rev. Immunol.* **6**, 595–601 (2006).
65. I. Hara, Y. Takechi, A. N. Houghton, Implicating a role for immune recognition of self in tumor rejection: Passive immunization against the brown locus protein. *J. Exp. Med.* **182**, 1609–1614 (1995).
66. H. Gogas, J. Ioannovich, U. Dafni, C. Stavropoulou-Giokas, K. Frangia, D. Tsoutsos, P. Panagiotou, A. Polyzos, O. Papadopoulos, A. Stratigos, C. Markopoulos, D. Bafaloukos, D. Pectasides, G. Fountzilas, J. M. Kirkwood, Prognostic significance of autoimmunity during treatment of melanoma with interferon. *N. Engl. J. Med.* **354**, 709–718 (2006).
67. S. L. Hewitt, D. Bailey, J. Zielinski, A. Apte, F. Musenge, R. Karp, S. Burke, F. Garcon, A. Mishra, S. Gurumurthy, A. Watkins, K. Arnold, J. Moynihan, E. Clancy-Thompson, K. Mulgrew, G. Adjei, K. Deschler, D. Potz, G. Moody, D. A. Leinster, S. Novick, M. Sulikowski, C. Bagnall, P. Martin, J.-M. Lapointe, H. Si, C. Morehouse, M. Sedic, R. W. Wilkinson, R. Herbst, J. P. Frederick, N. Luheshi, Intratumoral IL12 mRNA therapy promotes TH1 transformation of the tumor microenvironment. *Clin. Cancer Res.* **26**, 6284–6298 (2020).
68. S. K. Watkins, N. K. Egilmez, J. Suttles, R. D. Stout, IL-12 rapidly alters the functional profile of tumor-associated and tumor-infiltrating macrophages in vitro and in vivo. *J. Immunol.* **178**, 1357–1362 (2007).
69. E. J. Wherry, M. Kurachi, Molecular and cellular insights into T cell exhaustion. *Nat. Rev. Immunol.* **15**, 486–499 (2015).
70. B. C. Miller, D. R. Sen, R. Al Abosy, K. Bi, Y. V. Virkud, M. W. LaFleur, K. B. Yates, A. Lako, K. Felt, G. S. Naik, M. Manos, E. Gjini, J. R. Kuchroo, J. J. Ishizuka, J. L. Collier, G. K. Griffin, S. Maleri, D. E. Comstock, S. A. Weiss, F. D. Brown, A. Panda, M. D. Zimmer, R. T. Manguso, F. S. Hodi, S. J. Rodig, A. H. Sharpe, W. N. Haining, Subsets of exhausted $CD8^+$ T cells differentially mediate tumor control and respond to checkpoint blockade. *Nat. Immunol.* **20**, 326–336 (2019).

71. E. Y. Lin, J. G. Jones, P. Li, L. Zhu, K. D. Whitney, W. J. Muller, J. W. Pollard, Progression to malignancy in the polyoma middle T oncoprotein mouse breast cancer model provides a reliable model for human diseases. *Am. J. Pathol.* **163**, 2113–2126 (2003).
72. S. Spranger, R. Bao, T. F. Gajewski, Melanoma-intrinsic β-catenin signalling prevents anti-tumour immunity. *Nature* **523**, 231–235 (2015).
73. J. Deckers, T. Anbergen, A. M. Hokke, A. de Dreu, D. P. Schrijver, K. de Bruin, Y. C. Toner, T. J. Beldman, J. B. Spangler, T. F. A. de Greef, F. Grisoni, R. van der Meel, L. A. B. Joosten, M. Merkx, M. G. Netea, W. J. M. Mulder, Engineering cytokine therapeutics. *Nat. Rev. Bioeng.* **1**, 286–303 (2023).
74. I. Melero, E. Castanon, M. Alvarez, S. Champiat, A. Marabelle, Intratumoural administration and tumour tissue targeting of cancer immunotherapies. *Nat. Rev. Clin. Oncol.* **18**, 558–576 (2021).
75. I. Sagiv-Barfi, D. K. Czerwinski, S. Levy, I. S. Alam, A. T. Mayer, S. S. Gambhir, R. Levy, Eradication of spontaneous malignancy by local immunotherapy. *Sci. Transl. Med.* **10**, eaan4488 (2018).
76. P. F. Ferrucci, L. Pala, F. Conforti, E. Cocorocchio, Talimogene Laherparepvec (T-VEC): An intralesional cancer immunotherapy for advanced melanoma. *Cancers* **13**, 1383 (2021).
77. A. P. Algazi, C. G. Twitty, K. K. Tsai, M. Le, R. Pierce, E. Browning, R. Hermiz, D. A. Canton, D. Bannavong, A. Oglesby, M. Francisco, L. Fong, M. J. Pittet, S. P. Arlauckas, C. Garris, L. P. Levine, C. Bifulco, C. Ballesteros-Merino, S. Bhatia, S. Gargosky, R. H. I. Andtbacka, B. A. Fox, M. D. Rosenblum, A. I. Daud, Phase II trial of IL-12 plasmid transfection and PD-1 blockade in immunologically quiescent melanoma. *Clin. Cancer Res.* **26**, 2827–2837 (2020).
78. B. A. Carneiro, D. Zamarin, T. Marron, I. Mehmi, S. P. Patel, V. Subbiah, A. El-Khoueiry, D. Grand, K. Garcia-Reyes, S. Goel, P. Martin, J. Wang, Y. Wu, S. Eck, B. Ridgway, N. Elgeioushi, J. Eyles, N. Durham, A. Azaro, O. Hamid, Abstract CT183: First-in-human study of MEDI1191 (mRNA encoding IL-12) plus durvalumab in patients (pts) with advanced solid tumors. *Cancer Res.* **82**, CT183 (2022).
79. M. L. Telli, H. Nagata, I. Wapnir, C. R. Acharya, K. Zablotsky, B. A. Fox, C. B. Bifulco, S. M. Jensen, C. Ballesteros-Merino, M. H. Le, R. H. Pierce, E. Browning, R. Hermiz, L. Svenson, D. Bannavong, K. Jaffe, J. Sell, K. M. Foerter, D. A. Canton, C. G. Twitty, T. Osada, H. K. Lyerly, E. J. Crosby, Intratumoral plasmid IL12 expands $CD8^+$ T cells and induces a CXCR3 gene signature in triple-negative breast tumors that sensitizes patients to anti–PD-1 therapy. *Clin. Cancer Res.* **27**, 2481–2493 (2021).
80. K. H. Kim, H. K. Kim, H.-D. Kim, C. G. Kim, H. Lee, J. W. Han, S. J. Choi, S. Jeong, M. Jeon, H. Kim, J. Koh, B. M. Ku, S.-H. Park, M.-J. Ahn, E.-C. Shin, PD-1 blockade-unresponsive human tumor-infiltrating $CD8^+$ T cells are marked by loss of CD28 expression and rescued by IL-15. *Cell. Mol. Immunol.* **18**, 385–397 (2021).

Acknowledgments: We are grateful to M. Makris (College of Veterinary Medicine, Virginia Tech) for help on flow cytometry. **Funding:** This work was supported by the Jeffress Trust Awards and the National Science Foundation (CHE-1807911 to R.T.). **Author contributions:** Conceptualization: L.N. and R.T. Methodology: L.N., E.J., A.L.C., W.W., W.C., and R.T. Investigation: L.N., E.J., A.L.C., W.W., W.C., and R.T. Visualization: L.N., Z.H., and R.T. Supervision: R.T. Writing—original draft: L.N. and R.T. Writing—review and editing: L.N. and R.T. **Competing interests:** The authors declare that they have no competing interests. **Data and materials availability:** All data needed to evaluate the conclusions in the paper are present in the paper and/or the Supplementary Materials (data are accessible through the Virginia Tech Data Repository at https://doi.org/10.7294/25315681).

Submitted 9 September 2023
Accepted 19 March 2024
Published 19 April 2024
10.1126/sciadv.adk7695